eScience 2 (2022) 573–590

Contents lists available at ScienceDirect

eScience

journal homepage: www.keaipublishing.com/en/journals/escience

Review

Electrolyte design for rechargeable anion shuttle batteries

Yao Wang [a], Xu Yang [b], Zhijia Zhang [b], Xia Hu [a], Yuefeng Meng [a], Xia Wang [c], Dong Zhou [a,*], Hao Liu [b], Baohua Li [a,*], Guoxiu Wang [b,*]

[a] Tsinghua Shenzhen International Graduate School, Tsinghua University, Shenzhen 518055, China

[b] Centre for Clean Energy Technology, School of Mathematical and Physical Sciences, Faculty of Science, University of Technology Sydney, Sydney, NSW 2007, Australia

[c] Max-Planck-Institute for Chemical Physics of Solids, Topological Catalysis Group, Nöthnitzer Straße 40, 01187 Dresden, Germany

HIGHLIGHTS

- The working mechanisms, achievements, and challenges in developing anion shuttle battery (ASBs) electrolytes are reviewed.
- The unique properties and basic principles for designing ASB electrolytes are described and illustrated.
- Future perspectives on strategies to design electrolytes for ASBs are presented to facilitate grid-scale applications.

GRAPHICAL ABSTRACT

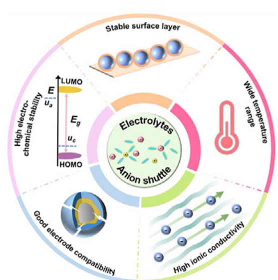

ARTICLE INFO

Keywords:
Anion shuttle batteries
Electrolytes
Electrochemical stability
Interfacial compatibility
Grid-scale energy storage

ABSTRACT

As an emerging new type of battery chemistry, the anion shuttle battery (ASB), based on the shuttling and storage of anions, is considered a sustainable alternative to gigawatt-scale energy storage due to the associated resource abundance, low cost, high safety, and high energy density. Although significant progress has been achieved, practical applications of ASBs are still hindered by tough challenges, such as short lifetime, limited reversible capacity, and low Coulombic efficiency. Therefore, it is very necessary to design and explore new electrolyte systems with high electrochemical/chemical stability, sufficient compatibility towards electrodes, and excellent kinetics/reversibility for anion electrochemical reactions. Here, we review the recent achievements and main challenges in developing electrolytes for ASBs, which include solid, non-aqueous, and aqueous electrolytes. We mainly focus on the unique properties and basic principles of designing these electrolytes, and their various performance parameters. Perspectives on design strategies for ASB electrolytes are also presented, which could facilitate the development of advanced ASBs for grid-scale energy storage.

1. Introduction

The current worldwide energy economy still relies heavily on fossil fuels, which causes severe air pollution and global warming. Motivated by the ever-increasing demands for renewable energy and its extensive applications, from portable electronics to grid storage, it is of vital significance to develop highly efficient energy storage and conversion technologies, such as rechargeable batteries [1,2]. Owing to their high energy density and long lifespan, lithium-ion batteries (LIBs) have come to dominate the battery markets, from portable electronics to electric vehicles [3,4]. However, the high cost and limited reserves of lithium and transition metals (e.g., Co, Ni) strongly hinder their applications for stationary energy

* Corresponding authors.
E-mail addresses: zhou.d@sz.tsinghua.edu.cn (D. Zhou), libh@sz.tsinghua.edu.cn (B. Li), Guoxiu.Wang@uts.edu.au (G. Wang).

https://doi.org/10.1016/j.esci.2022.10.003
Received 25 July 2022; Received in revised form 6 October 2022; Accepted 17 October 2022
Available online 21 October 2022

storage [5]. Alternative rechargeable metal-ion batteries based on other univalent or multivalent cations as charge carriers (e.g., Na^+, Ca^{2+}, Mg^{2+}, Zn^{2+}, Al^{3+}) have been developed [6,7]. However, their large ionic radii mean they suffer from limited energy density and/or significant challenges when it comes to ion transport and reversible cycling, which makes them less competitive for widespread applications.

Recently, a new type of battery chemistry based on the shuttling and storage of anions (e.g., Cl^-, F^-, $NO_3{}^-$, $PF_6{}^-$, $TFSI^-$, FSI^-) has attracted increasing attention due to low cost, resource abundance, safety, and high energy/power density. In contrast to cation rocking-chair batteries (CRBs, e.g., LIB), where the cations are transported between cathode and anode upon charging/discharging, anion shuttle batteries (ASBs) utilize anions as the principal charge carriers for electrochemical reactions [8,9].

ASBs can be divided into three configurations: (i) anion rocking-chair batteries (ARBs), e.g., chloride-ion batteries (CIBs) and fluoride-ion batteries (FIBs), which rely on the shuttling of anions between the two electrodes for charge storage; specifically, anions are released from the cathode and transfer to the anode upon discharging, while the process occurs in reverse during the charge process [8–10]; (ii) dual-ion batteries (DIBs), which exhibit a different operating mechanism involving the simultaneous incorporation of anions and cations into the cathode and the anode, respectively, during charging, and the simultaneous release of the charge carriers into the electrolyte during discharging (Fig. 1c) [11,12]; (iii) analogous to DIBs, reverse dual-ion batteries (RDIBs) utilize both cations and anions for the energy storage process, with anions being incorporated into the anode and cations into the cathode upon discharging, while in the subsequent charge process, both ions return to the electrolyte simultaneously [13].

Generally, the unique features of anions as charge carriers give ASBs key advantages, such as high energy density (theoretical energy density of 2500 Wh L^{-1} for CIBs and 5000 Wh L^{-1} for FIBs, respectively) and/or high power capability (with DIBs) [14–16]. In addition, ASBs utilize earth-abundant anions in place of Li^+ as the principal charge carrier, and their inexpensive electrode materials are effective for reducing manufacturing cost [10]. These merits facilitate the development of ASBs, which offer great potential for low-cost grid-scale energy storage. Thus far, however, our understanding of the relationship between anionic charge carriers and their electrochemical performance remains limited.

It is essential that ASB electrolytes comply with the same key requirements as LIBs: (i) high ionic conductivity to enable fast anion transport, and negligible electronic conductivity to suppress battery self-discharge; (ii) excellent chemical stability and inertness towards the cathode and anode materials, as well as the separator, current collector, and other cell packing components to mitigate side reactions; (iii) a wide electrochemical stability window (ESW), i.e., a large energy gap between the lowest unoccupied molecular orbital (LUMO) and the highest occupied molecular orbital (HOMO), to achieve high energy density and to prevent electrolyte side reactions within the cell operating voltage; (iv) low interfacial resistance to ensure good contact, and a low energy barrier for ionic conduction between the electrode and the electrolyte. These electrolyte properties play a decisive role in the kinetics/reversibility of

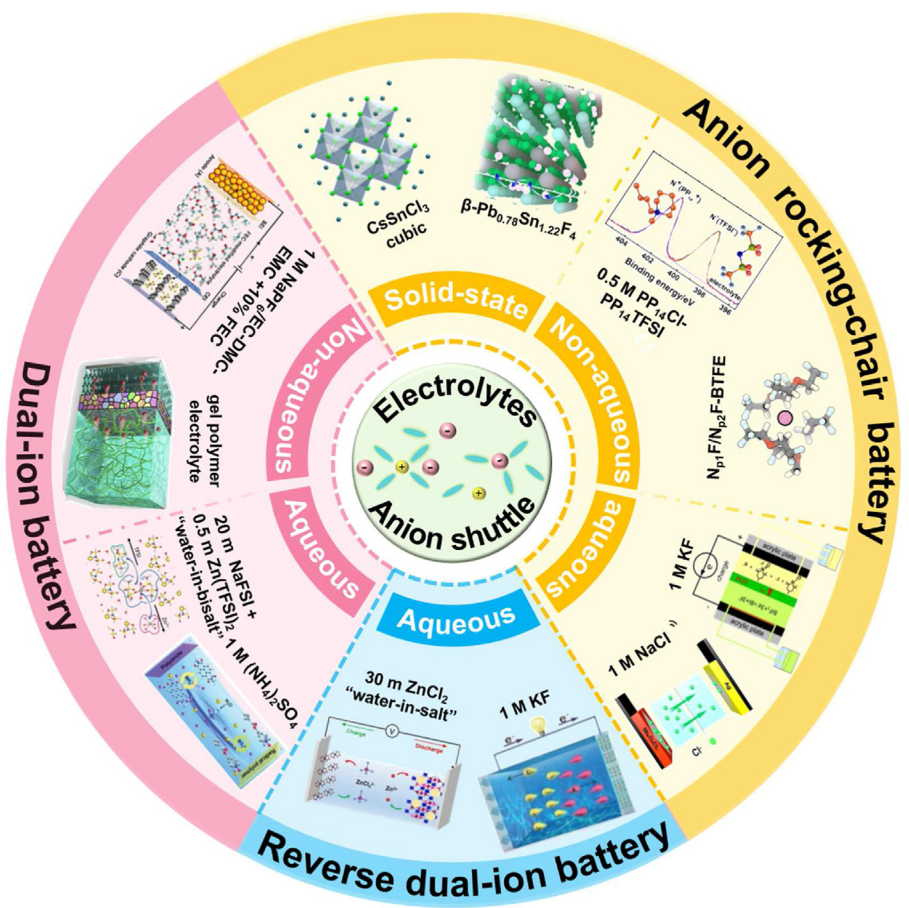

Fig. 1. Overview of electrolyte progress for anion rocking-chair batteries, dual-ion batteries, and reverse dual-ion batteries, including aqueous, non-aqueous, and solid-state electrolytes. Reproduced with permission [13,17]. Copyright 2019, American Chemical Society. Reproduced with permission [18,19]. Copyright 2021, Wiley-VCH. Reproduced with permission [20]. Copyright 2017, American Chemical Society. Reproduced with permission [21]. Copyright 2020, American Chemical Society. Reproduced with permission [22,23]. Copyright 2021, American Chemical Society. Reproduced with permission [24]. Copyright 2020, Elsevier. Reproduced with permission [25]. Copyright 2019, Royal Society of Chemistry. Reproduced with permission [26]. Copyright 2018, American Association for the Advancement of Science. Reproduced with permission [27]. Copyright 2019, The Electrochemical Society.

electrochemical reactions and the lifespan of ASBs. However, compared with the extensive studies on electrode materials (cathode and anode), research work and reviews on electrolyte development for ASBs are lacking [8–10,12,28–31].

Notably, the migrated anions in ARBs are initially stored in the cathode materials, and the electrolyte only serves as the charge carrier to transport anions, hence the ion concentration remains unchanged during the charge/discharge process. In contrast, for DIBs and RDIBs, since both the cations and the anions for charge transfer are supplied by the electrolyte, the ions in the electrolyte should be considered the active material. Consequently, in DIBs and/or RDIBs, the concentrations of both cations and anions, and the corresponding physical qualities of the electrolyte, such as ionic conductivity and viscosity, are highly dependent on the state of charge (SOC). Remarkably, the reversible capacity, energy/power density, and cell voltage of DIBs and/or RDIBs depend largely on the electrolyte formulation (e.g., the type of solvent, the salt type and content, the additive amount) [32].

In this review, we focus on discussing the recent achievements and main challenges in developing electrolytes — including solid, non-aqueous, and aqueous (Fig. 1) — for ARBs, DIBs, and RDIBs. The unique properties of each type of electrolyte (ESW, ionic transport, electrode/electrolyte compatibility, etc.) are summarized, and perspectives on future design strategies for ASB electrolytes are proposed.

2. Electrolytes for ARBs

ARBs function based on anion shuttling across cathodes and anodes for electrochemical reactions during charging/discharging, two representative examples being CIBs and FIBs. In general, these batteries utilize a metal as the anode and a metal halide or metal halide-containing material as the cathode. As mentioned in the introduction, the rich abundance of halide materials makes far less expensive redox pairs in ARBs than in LIBs. More interestingly, the wide range of possible redox pairs and/or multiple-electron transfer reactions can potentially yield extremely high energy densities for ARBs. However, several major obstacles remain, one crucial factor being the need for a suitable electrolyte design that achieves high ionic conductivity, superb interfacial stability, as well as stable/reversible charge storage reactions. This will be comprehensively discussed in the following section.

2.1. Chloride-ion batteries (CIBs)

The first proof-of-concept CIB based on Cl^- shuttling through a Cl^--containing electrolyte was proposed by Fichtner et al., in 2014, and since then, the CIB has attracted intensive attention owing to its high theoretical volumetric energy density, low cost, dendrite-free operation, and other features [33–35]. In particular, the massive abundance of Cl^--containing materials allows a wide array of potential redox pairs, giving CIBs a theoretical energy density comparable to that of lithium–sulfur batteries (~2800 Wh L^{-1}) [35]. As the charge carrier across the cathode and anode, the electrolyte plays a critical role in CIB performance, such as cyclability. Two of the biggest challenges for developing CIB electrolytes lie in providing fast Cl^- anion conduction and superior electrode compatibility at room temperature (RT). The key progress and main challenges for state-of-the-art CIB electrolytes will be discussed in detail below.

2.1.1. Solid electrolytes

Solid electrolytes have been demonstrated to be effective in solving issues associated with electrode dissolution and/or undesirable side reactions between electrode materials and liquid electrolytes, and they are garnering increasing interest in the field of LIB systems. Nevertheless, only a few studies have been reported on chloride-ion-conducting solid electrolytes for CIBs [21,36,37]. Zhao et al. developed the first all-solid-state rechargeable CIB by employing a ternary solid electrolyte, which consisted of a poly(ethylene oxide) (PEO) matrix, a quaternary ammonium chloride salt (TBMACl), and a succinonitrile (SN) solid plasticizer. The PEO_1-$TBMACl_1$-SN_3 solid electrolyte exhibited a high anti-oxidation stability of more than 4.2 V vs. Li/Li^+ and a conductivity of 10^{-5}–10^{-4} S cm^{-1} within the temperature range of 198–343 K. Consequently, a FeOCl (cathode)||Li (anode) battery using this electrolyte displayed reversible redox reactions during charging/discharging (Figs. 2a–c) [36].

Inorganic compounds such as $BaCl_2$, $SrCl_2$, and LaOCl can also be utilized as chloride-ion conductors. However, the ionic conductivity (~10^{-6} S cm^{-1}) of these polycrystalline materials can only be achieved at an operating temperature above 500 K [38,39]. Some metal chlorides, such as $SnCl_2$-and $PbCl_2$-based materials, have exhibited enhanced ionic conductivities (~10^{-6} S cm^{-1}) at RT, but they suffered from reduced electrochemical reduction stability [40,41]. Zhao et al. reported a room-temperature-stable inorganic halide perovskite of $CsSnCl_3$ prepared by mechanical milling and subsequent mild heat treatment, which demonstrated highly enhanced structural stability against phase transformation of the cubic structure (Fig. 2d), thus enabling a high ionic conductivity of 3.6×10^{-4} S cm^{-1} at RT together with a wide electrochemical window of ~6.1 V (Fig. 2e) [21]. Although remarkable progress has been made, extensive efforts are still needed to enhance the Cl^- ion conductivity and/or interfacial properties of solid electrolytes, such as by structurally engineering inorganic chloride ion conductors (e.g., doping), to achieve solid CIBs that operate at room temperature.

2.1.2. Non-aqueous liquid electrolytes

Compared with solid electrolytes, the high ionic conductivities of non-aqueous liquid electrolytes enable the operation of rechargeable CIBs at RT. Since their first development in 2014, the majority of rechargeable CIBs have been explored based on non-aqueous electrolytes (Table 1) comprising mixtures of ionic liquids (IL) and/or carbonates as solvents.

A binary IL electrolyte was designed by mixing 1-methyl-3-octylimidazolium chloride ([OMIM][Cl]), possessing low melting point but high viscosity, with 1-butyl-3-methylimidazolium tetrafluoroborate ([BMIM][BF_4]) in a 1:3 volume ratio, which accelerated the movement of Cl^- ions. Owing to the combined merits of the two ILs, reversible Cl^- transfer was achieved at RT, contributing to a high discharge capacity of 142.9 mAh g^{-1} for a $BiCl_3$||Li cell based on the mass of $BiCl_3$ [33]. To further improve the Cl^- ionic conductivity/mobility, carbonates have been introduced into IL electrolytes as co-solvents. By dissolving 0.5 M 1-butyl-1-methylpiperidinium chloride (PP_{14}Cl) in propylene carbonate (PC) solvent, Fichtner and co-workers reported a novel electrolyte that demonstrated both a high ionic conductivity of 4.4 mS cm^{-1} and a wide electrochemical window of 3.2 V versus Li/Li^+. Coupling this electrolyte with a VOCl cathode and a Li anode, an initial discharge capacity of 189 mAh g^{-1} at 2 C based on the active material of the cathode was achieved for the CIB, which retained a high discharge capacity (113 mAh g^{-1}) even after 100 cycles (Figs. 3a and b) [43]. Han et al. developed a highly reversible CIB comprising $Ni_2V_{0.9}Al_{0.1}$-Cl layered double hydroxides (LDH) as the cathode and Li as the anode, and employing 1 M 1-butyl-1--methylpyrrolidinium chloride (BpyCl) in PC and 1-butyl-1-methylpiperidinium bis(trifluoromethylsulfonyl) imide (PP_{14}TFSI) as the electrolyte. Electrode dissolution was mitigated, contributing to a high capacity of 312.2 mAh g^{-1} and an ultralong lifetime of 1000 cycles, with a stable capacity of 113.8 mAh g^{-1} based on the mass of the cathode material [45].

Although these IL-based electrolytes have been regarded as a possible choice for CIB applications due to the high Cl^- ionic conductivity and wide ESW, they generally suffer from serious interfacial side reactions (e.g., electrode dissolution into the electrolytes) and carry high risks of leakage, volatility, and flammability. To resolve these issues, gel polymer electrolytes were developed as potential candidates for rechargeable CIBs. Gschwind et al. reported three types of Cl^--conducting polymer electrolytes that combined the polymer with chloride salts containing large cations — tetraethyl ammonium chloride with gelatin, tetrabutyl ammonium chloride (TBACl) with polyvinyldifluoride-hexafluoropolymer (PVDF-HF),

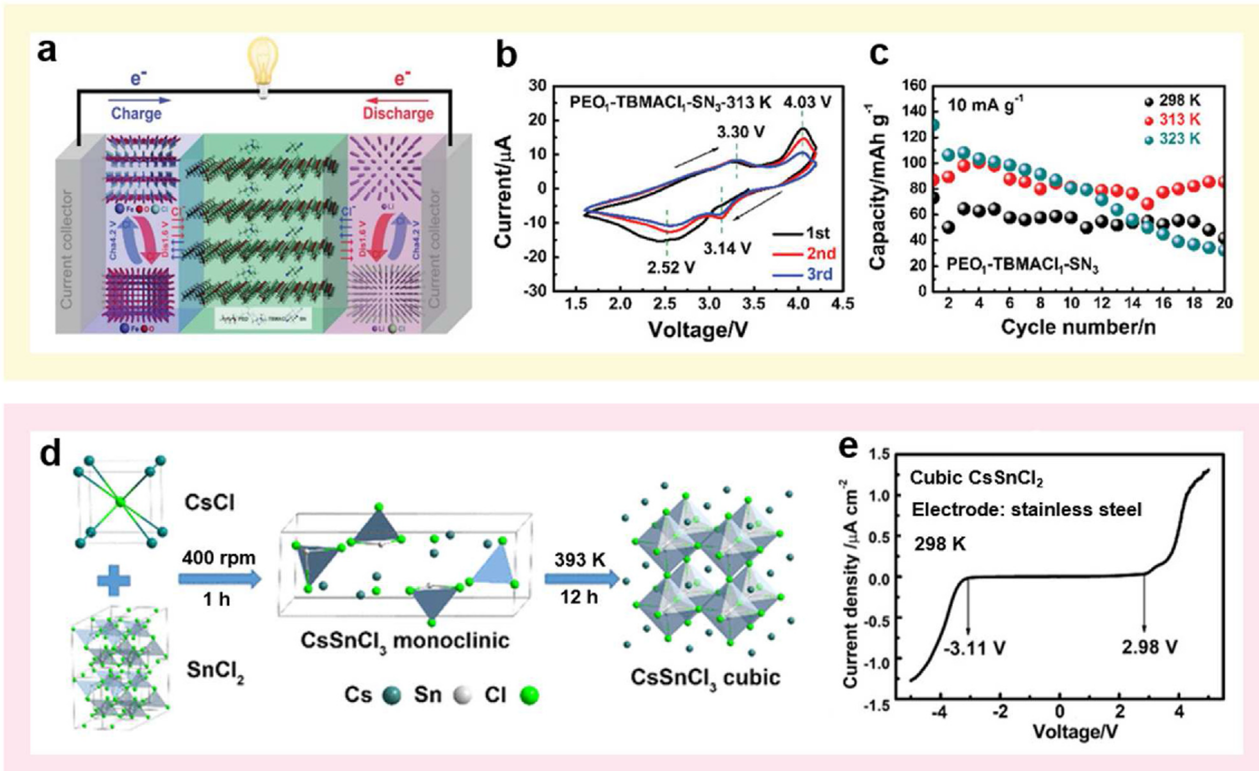

Fig. 2. Solid electrolytes for CIBs. (a) Schematic diagram, (b) cyclic voltammetry (CVs, 50 μV s^{-1}), and (c) cycle performance (10 mA g^{-1}) of a FeOCl|PEO_1-$TBMACl_1$-SN_3|Li cell. Reproduced with permission [36]. Copyright 2019 Wiley-VCH. (d) Schematic of the preparation of $CsSnCl_3$ perovskite solid-state electrolyte. (e) Linear sweep voltammetry (LSV) of the cubic $CsSnCl_3$ electrolyte at 298 K with a scan rate of 5 mV s^{-1}, demonstrating an electrochemical stability window of ~6.1 V. Reproduced with permission [21]. Copyright 2020, American Chemical Society.

and octyltrimethyl ammonium chloride (TOACl) with polyvinylchloride (PVC), respectively [49]. The PVC-based electrolyte displayed the lowest ionic conductivity of 10^{-7} S cm^{-1}, whereas the other two electrolytes showed higher conductivity (10^{-4} S cm^{-1}). However, the Cl^- conductivities of these polymer electrolytes were lower compared to IL-based electrolytes, and electrochemical processes only occurred at the electrode/electrolyte interface. In addition, although these electrolytes were combined with a Zn anode and a $CuCl_2$, $BiCl_3$, or polyaniline (PANI) cathode, respectively, as prototype batteries, only discharge performance was reported, while their reversibility was doubtful. Further studies of the stability/reversibility of the electrochemical reactions upon charging/discharging with improved battery setups are therefore urgently required.

Immobilization of Cl-containing ILs within polymer matrices can be another effective approach, forming IL-based polymer electrolytes that have high ionic conductivity as well as enhanced thermal and electrochemical stability. Such IL-based polymer electrolytes exhibit rather better electrode compatibility compared with solid electrolytes. Recently, a Cl^--conducting IL-based polymer electrolyte based on cross-linked poly(methyl methacrylate) (PMMA)-0.5 M $PP_{14}Cl$-$PP_{14}TFSI$ was demonstrated, where the IL acted as both plasticizer and Cl^- supplier. When containing 80 wt% ILs, the IL-based polymer electrolyte exhibited a high ionic conductivity of 0.90×10^{-4} S cm^{-1} and a high anodic stability limit of 5.0 V (using stainless steel as the counter electrode) at RT. An as-assembled FeOCl|PMMA-0.5 M $PP_{14}Cl$-$PP_{14}TFSI$|Li cell yielded a high discharge capacity of 122 mAh g^{-1} based on the mass of FeOCl after 7 cycles at 10 mA g^{-1}, demonstrating the application feasibility of Cl^--conducting IL-based polymer electrolytes for high-performance CIBs [47].

2.1.3. *Aqueous electrolytes*

In addition to non-aqueous electrolytes containing ILs or organic solvents, aqueous electrolytes have also been explored in rechargeable CIBs, displaying obvious advantages that include nonflammability, eco-friendliness, safety, and low cost due to the facile fabrication process [8,9,14]. However, most electrode materials for CIBs suffer from significant dissolution or stability issues in aqueous electrolytes. In addition, the narrow stability window of the electrolyte solvent, i.e. water, restricts the battery energy density. By pairing a silver cathode with a BiOCl anode, Yang et al. demonstrated the first aqueous CIB by using 1 M NaCl as an electrolyte [14]. This aqueous CIB exhibited obvious redox peaks representing Cl^- insertion and extraction between the two electrodes, leading to a stable discharge capacity of 92.1 mAh g^{-1} (based on the mass of the BiOCl anode) that was maintained for 45 cycles at a current density of 400 mA g^{-1} (Fig. 3c) [14]. After that, Sun et al. replaced the anode material with $Sb_4O_5Cl_2$, and the resulting Ag||$Sb_4O_5Cl_2$ full battery (Fig. 3d) using 1 M NaCl electrolyte demonstrated a discharge capacity of 34.6 mAh g^{-1} (based on the mass of $Sb_4O_5Cl_2$) after 50 cycles at 600 mA g^{-1} [17]. In another effort to address the poor stability and volume expansion/contraction for the conversion reaction between Bi and BiOCl during the electrochemical process, a Bi-nanoparticle@carbon-film composite electrode was employed as an anode. When this anode was coupled with a AgCl cathode and NaCl electrolyte, a high capacity of 87.9 mAh g^{-1} based on the Bi weight was achieved after 200 cycles at 400 mA g^{-1} [48]. Nevertheless, the aqueous CIBs reported thus far have relied on NaCl as the chloride salt. Other chloride salts and/or highly concentrated electrolytes (HCEs) should be explored to enhance the electrolyte electrochemical window and further improve the compatibility/stability of the electrode materials towards aqueous electrolytes.

2.2. *Fluoride-ion batteries (FIBs)*

Similar to CIBs, the rechargeable FIB operated by a F^- shuttle has emerged as a competitive battery technology that is attracting increasing attention. Owing to the high electronegativity of F, the F^- anion exhibits superb anti-oxidation stability, which enables the utilization of high-

Table 1
Comparison of the electrochemical performance of non-aqueous and aqueous electrolytes for CIBs.

Electrolyte	Cathode||Anode	Output voltage (V)	Specific capacity (mAh g^{-1})	Retained capacity (mAh g^{-1})/ cycles	Ref.
0.5 M $PP_{14}Cl$-$PP_{14}TFSI$	FeOCl||Li	1.6–3.5	158 at 10 mA g^{-1}	60/30	[35]
0.5 M $N_{116(14)}Cl$-$N_{1114}TFSI$	BiOCl||Li	1.6–3.0	60 at 5 mA g^{-1}	60/6	[35]
0.5 M $PP_{14}Cl$-$PP_{14}TFSI$	FeOCl/CMK-3|| Li	1.6–3.5	202 at 10 mA g^{-1}	162/30	[42]
0.5 M $PP_{14}Cl$-$PP_{14}TFSI$	PPyCl@CNTs || Li	1.0–4.0	118 at 500 mA g^{-1}	~90/40	[20]
[OMIM][Cl]-[BMIM][BF_4] (1:3)	VCl_3||Li	1.6–3.5	111.8 at 3 mA g^{-1}	–	[33]
[OMIM][Cl]-[BMIM][BF_4] (1:3)	$BiCl_3$||Li	1.6–3.5	142.9 at 3 mA g^{-1}	~80/3	[33]
0.5 M $PP_{14}Cl$- PC	VOCl||Li	1.0–2.8	151 at 522 mA g^{-1}	113/100	[43]
0.5 M BpyCl-PC/ $PP_{14}TFSI$	CoFe–Cl LDH|| Li	1.2–3.0	239.3 at 100 mA g^{-1}	160/100	[44]
0.5 M BpyCl-PC/ $PP_{14}TFSI$	$Ni_2V_{0.9}Al_{0.1}$–Cl LDH||Li	1.2–3.0	312 at 200 mA g^{-1}	113.8/ 1000	[45]
0.5 M $Bpy_{14}Cl$-PC	NiFe–Cl LDH||Li	1.2–3.0	350.6 at 100 mA g^{-1}	101.1/800	[46]
PMMA-0.5 M $PP_{14}Cl$-$PP_{14}TFSI$	FeOCl||Li	1.6–3.5	~122 at 10 mA g^{-1}	122/7	[47]
1 M NaCl	Ag||BiOCl	0–1.5	153 at 400 mA g^{-1}	92.1/45	[14]
1 M NaCl	Ag||$Sb_4O_5Cl_2$	0–1.5	41 at 600 mA g^{-1}	34.6/50	[17]
1 M NaCl	AgCl|| Bi@carbon-texture	0–1.2	94.2 at 400 mA g^{-1}	87.9/200	[48]

Note: Benzyldimethyltetradecylammonium chloride ($N_{116(14)}Cl$); Butyltrimethylammonium bis(trifluoromethyl-sulfonyl)imide ($N_{1114}TFSI$).

voltage redox couples [9,10,50]. In addition, the multiple-electron electrochemical reactions for F^- storage are promising for achieving high theoretical energy density [50]. Compared to the use of Cl^- as the charge carrier in CIBs, the smaller size and lower weight of the F^- anion enables faster ionic transport and higher energy density for FIBs [10,51]. Although research into rechargeable FIBs is in the fledgling stage, electrolyte design and related mechanism studies have been a significant research area, especially in recent years [52–57]. In the following section, we will provide an overview of the current F^--transporting solid and liquid electrolytes suitable for the efficient functioning of FIBs.

2.2.1. Solid electrolytes

The first proof-of-principle rechargeable FIB was demonstrated by Fichtner et al., in 2011 and employed $La_{0.9}Ba_{0.1}F_{2.9}$ as a F^- ion-conducting solid electrolyte, achieving a high ionic conductivity of $\sim 2.0 \times 10^{-4}$ S cm^{-1} at 150 °C [50]. When combined with a BiF_3/Ce redox couple, a discharge capacity of 190 mAh g^{-1} based on the mass of BiF_3 was delivered for the initial cycle. However, due to the large volume change in electrode materials and the consequent loss of electrode–electrolyte contact upon repeated charging/discharging, the cell suffered from poor cycling stability. Following this pioneering work, numerous reports exploring solid electrolytes for FIBs have appeared [52, 55,56,58–62]. In solid electrolytes, ionic transport is mainly achieved via Schottky and anti-Frenkel point defects (i.e., the vacancy mechanism, interstitial mechanism, and interstitial-substitutional exchange mechanism). Therefore, creating more defects in the solid structure can enhance ionic conductivity [31]. Typically, F^--ion transporting solid electrolytes are categorized into two types: alkaline-earth fluorides with a fluorite-type structure (MF_2, M = Ba, Ca, Sr) and rare-earth fluorides with a tysonite-type structure (MF_3, M = La, Ce, Pr, Nd) [63,64]. However, some of these solid electrolytes can achieve high ionic conductivity without a high concentration of defects.

Owing to the lone pair of electrons on the Sn^{2+} atom, SnF_2-containing compounds (e.g., $MSnF_4$, M = Pb, Ba, Ca, etc.) have been reported to possess high ionic conductivity. The polarizable lone pair can reorient while moving, and the mobile F^- between Sn–Sn and Sn–Ba layers thus can participate in the conduction process, leading to an enhanced ionic conductivity from 2×10^{-10} S cm^{-1} at 160 °C for BaF_2 to above 1×10^{-4} S cm^{-1} at RT for $BaSnF_4$ solid electrolytes [31,53]. Unfortunately, the low electrochemical stability of Sn^{2+} has largely restricted the application of highly reductive electrode materials. On the other side, the widely studied tysonite-type $La_{0.9}Ba_{0.1}F_{2.9}$ displayed low ionic conductivity (4×10^{-7} S cm^{-1} at RT), while it was compatible towards metal anodes like Ce and La. To combine advantages from both electrolytes, Mohammad et al. pressed together a thick $BaSnF_4$ layer with a thin $La_{0.9}Ba_{0.1}F_{2.9}$ layer. The resulting interlayer electrolyte achieved a much higher ionic conductivity (8.9×10^{-6} S cm^{-1}) than $La_{0.9}Ba_{0.1}F_{2.9}$ electrolyte on its own (4.0×10^{-7} S cm^{-1}) while also preventing physical contact between the less stable $BaSnF_4$ and the anode. This interlayer electrolyte enabled a BiF_3||Ce battery to be charged/discharged at RT, though the first discharge capacity (only 27 mAh g^{-1}) decayed rapidly [54].

To further demonstrate that lone pairs could improve electrolyte ionic conductivity, Reddy et al. substituted trivalent Sb^{3+} for divalent Ba^{2+}, revealing that the fluorite-type structured $Ba_{1-x}Sb_xF_{2+x}$ ($0.1 \le x \le 0.4$) solid conductors displayed enhanced ionic conductivities (Figs. 4a and b) [64]. The migration of fluoride vacancies along the grain boundaries accounts for the ionic conductivity of $Ba_{1-x}Sb_xF_{2+x}$ compounds, wherein the lone pair of electrons on Sb^{3+} appear to facilitate the F^- mobility. Though the highest ionic conductivity (4.4×10^{-4} S cm^{-1} at 160 °C) was obtained with $Ba_{0.7}Sb_{0.3}F_{2.3}$ solid electrolyte, insufficient evidence was provided to determine the role of lone pairs in improving the ionic conductivity.

In the case of tysonite-type fluorides ($R_{1-x}M_xF_{3-x}$, where R is the rare-earth element and M is the divalent element), a F^- interstitial site cannot be formed because it is much smaller (0.84 Å) than the F^- radius (1.19 Å). The ionic conductivity of tysonite-type fluorides can be improved via creating F^- vacancies in RF_3 [65]. Fichtner et al. investigated the conduction mechanism of a $La_{1-y}Ba_yF_{3-y}$ ($0 \le y \le 0.15$) solid compound synthesized by mechanical milling, revealing that the mechanism of conductivity was rather different from that of fluorite-type structured compounds (Figs. 4c and d) [61]. In contrast to the dominant role played by the migration of vacancies along the grain boundaries in the ionic conductivity of fluorite-type compounds ($Ba_{1-x}La_xF_{2+x}$), the grain boundaries had detrimental impacts on ionic conduction for tysonite-type compounds ($La_{1-y}Ba_yF_{3-y}$). Sintering of the $La_{0.9}Ba_{0.1}F_{2.9}$ compound led to grain growth and a reduction in grain boundaries, causing enhancement of the F^- ionic conductivity. This confirmed that the grain boundaries acted as a barrier to conduction; however, the exact contribution of grain boundaries to ion conduction remains uncertain.

Reducing the thickness of electrolyte films has been recognized as another strategy to improve the ionic conductivity of solid electrolytes. A thick solid electrolyte layer (700–800 μm) typically results in high resistance for the ionic conductor and poor contact between the solid electrolyte and the electrodes, which can be mitigated by employing a thin-film mode (Fig. 4e). Preparing thin-film electrolytes of $La_{1-x}Ba_xF_{3-x}$ ($0 \le x \le 0.15$) by a sol-gel spin-coating method, Fichtner et al. achieved an ionic conductivity of 8.8×10^{-5} S cm^{-1} at 170 °C ($La_{0.9}Ba_{0.1}F_{2.9}$) [60]. In spite of the conductivity being lower than with bulk solid electrolytes

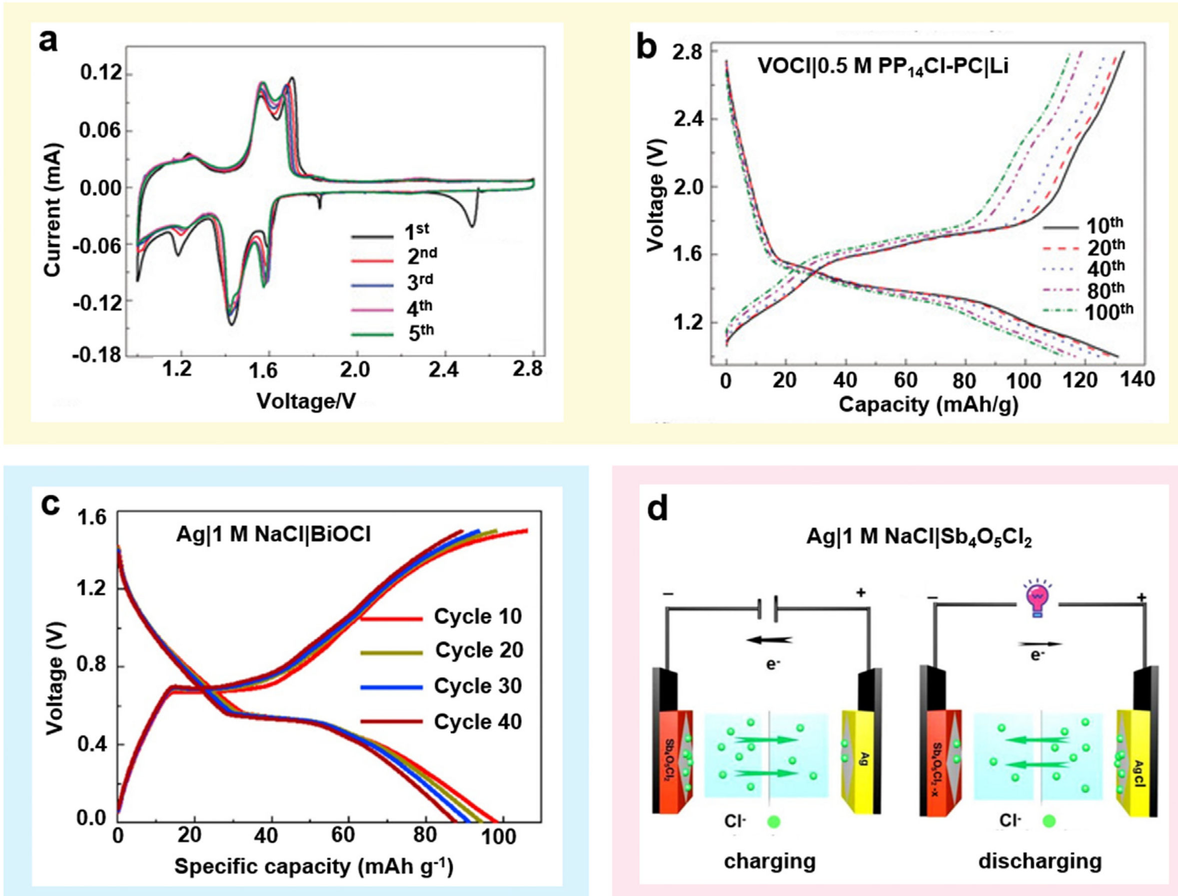

Fig. 3. Non-aqueous and aqueous electrolytes for CIBs. A non-aqueous VOCl|0.5 M $PP_{14}Cl$-PC|Li CIB with (a) CV measurements at a scan rate of 0.1 mV s^{-1} and (b) cycling performance at 2 C (1 C = 261 mA g^{-1}). Reproduced with permission [43]. Copyright 2016, Wiley-VCH. (c) Charge and discharge curves for an aqueous Ag|1 M NaCl|BiOCl CIB at a current density of 400 mA g^{-1}. Reproduced with permission [14]. Copyright 2017, Elsevier. (d) Schematic illustration of the working mechanism for an aqueous Ag|1 M NaCl|$Sb_4O_5Cl_2$ CIB. Reproduced with permission [17]. Copyright 2019, American Chemical Society.

synthesized by ball milling, the thin-film strategy reduced the overall resistance of the FIBs. Soon after, using $La_{0.9}Ba_{0.1}F_{2.9}$ as a thin-film electrolyte, Fichtner et al. achieved initial discharge capacities of 66 and 76 mAh g^{-1} based on the weight of the active material in the cathode at 160 °C for Bi||MgF_2 and Cu||MgF_2 FIBs, respectively. Nevertheless, the capacity for both cells faded sharply during subsequent cycles [66]. Very recently, a tetragonal β-$Pb_{0.78}Sn_{1.22}F_4$ thin film synthesized by pulsed laser deposition (PLD) was employed as a solid electrolyte for FIBs [22]. The ionic conductivity of the thin-film electrolyte was enhanced due to the regulation of preferential growth under various annealing atmospheres. The rate-determining factor of the interfacial reaction kinetics for solid-state FIBs was investigated (Fig. 4f), revealing that mass transfer (F^- conduction in electrolyte) should be the limiting process at the interface between an electrode and the thin-film electrolyte.

Solid electrolytes bring FIBs several obvious advantages, such as safety, high chemical stability, and a wide ESW. However, their high operating temperature (> 140 °C), low ionic conductivity, poor interfacial contact, and incompatibility with most conversion-type electrode materials are still tough challenges for the practical application of rechargeable solid FIBs.

2.2.2. Non-aqueous liquid electrolytes

Non-aqueous liquid electrolytes generally possess higher ionic conductivities than those of solid electrolytes. Unfortunately, due to the existence of lone pairs within the ionic radius, "naked" F^- ions are highly reactive with nucleophilicity and basicity. As a result, organic cations possessing β-hydrogens easily undergo Hoffman elimination and salt decomposition, posing a great challenge for designing stable liquid electrolytes in FIBs at RT [10]. Pioneering reports demonstrate that designing electrolytes that are resistive to nucleophilic F^- attack and solvating F^- with Lewis acidic agents to reduce its basicity are effective strategies for developing liquid fluoride electrolytes [51,67–69].

In 2017, dissolving 1 M organic fluoride (1-methyl-1-propylpiperidinium fluoride: MPPF) in ILs (*N,N,N*-trimethyl-*N*-propylammonium bis(trifluoromethanesulfonyl)-amide: TMPA/TFSI) as the F^--transporting electrolyte, Okazaki et al. produced a 0.35 M MPPF-TMPA/TFSI electrolyte with a high ionic conductivity of 2.5 mS cm^{-1} [70]. By combining this electrolyte with a Bi cathode and a PbF_2|Pb anode, a charge capacity of 1.2 mAh cm^{-2} was achieved with a Coulombic efficiency of ~56%. Nevertheless, organic cations with β-hydrogens in ILs were considered to potentially generate bifluoride ions, attributed to Hofmann elimination [9,65]. Despite such drawbacks, these reports were still pioneering in designing liquid electrolytes for room-temperature FIBs.

A significant advance in designing stable room-temperature F^--conducting electrolytes was achieved by Jones et al., in 2018 [51]. The electrolytes were prepared by dissolving tetraalkylammonium fluoride salts (i.e., neopentyl (Np)-substituted alkylammonium fluorides) in ethers. The solubility of the organic fluoride salt could be improved due to the branched Np chain, while the decomposition of F^- to HF_2^- could be suppressed in the absence of β-hydrogens. Bis(2,2,2-trifluoroethyl) ether (BTFE) was found to be the only organic solvent able to dissolve

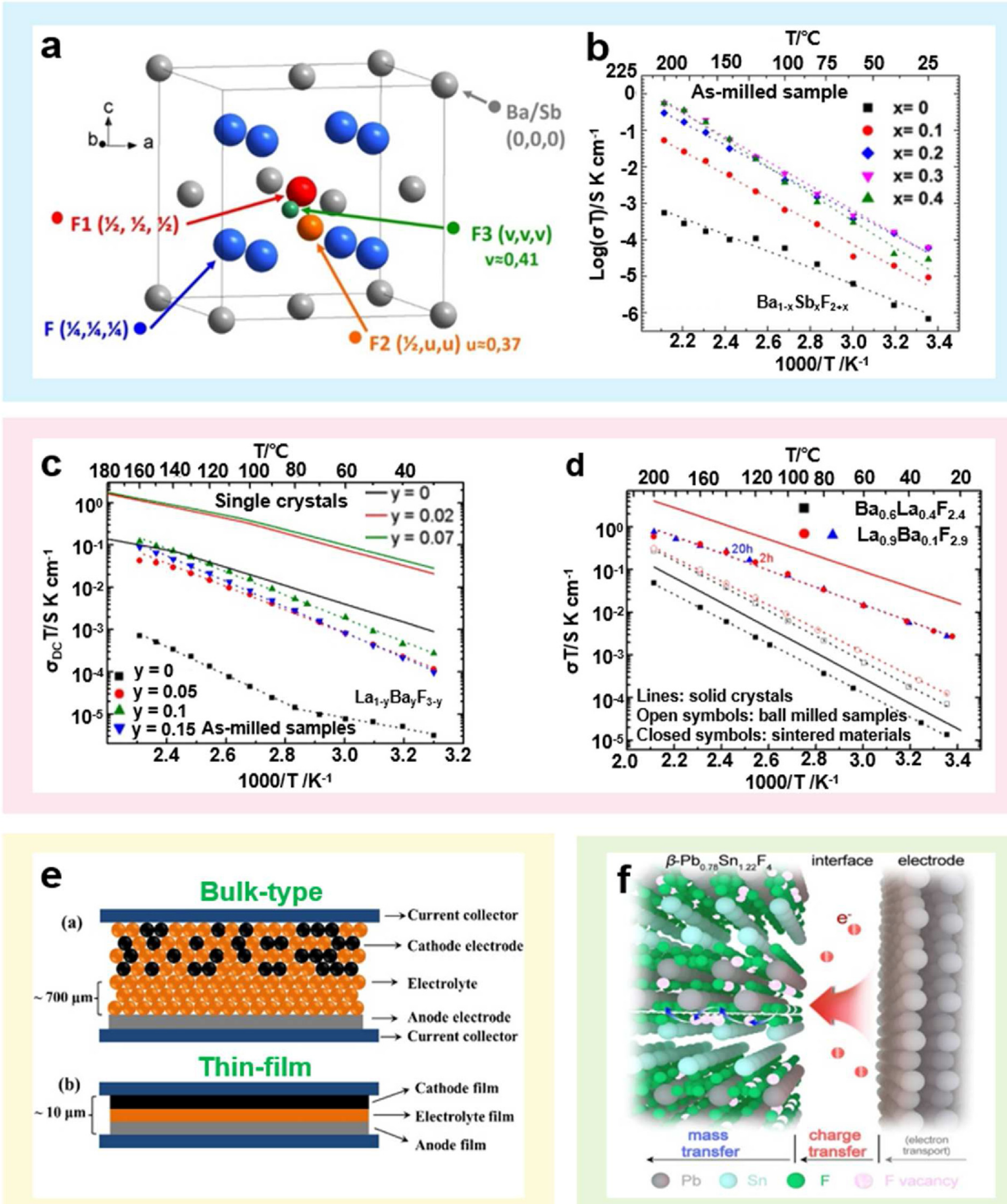

Fig. 4. Solid electrolytes for FIBs. (a) Representative structure of $Ba_{1-x}Sb_xF_{2+x}$ (doped fluorite). (b) Arrhenius plots of ionic conductivity of ball-milled $Ba_{1-x}Sb_xF_{2+x}$ ($0 \le x \le 0.4$) compounds. Conductivities were measured from impedance measurements, while the dotted lines represent the linear fitted results. Reproduced with permission [64]. Copyright 2018, American Chemical Society. (c) Arrhenius plot of the conductivity for $La_{1-y}Ba_yF_{3-y}$ electrolyte prepared by ball milling. (d) Arrhenius plots of the conductivities for ball-milled and sintered samples of tysonite-type $La_{0.9}Ba_{0.1}F_{2.9}$ and fluorite-type $Ba_{0.6}La_{0.4}F_{2.4}$. Reproduced with permission [61]. Copyright 2014, American Chemical Society. (e) Schematic illustrations of a bulk-type solid battery and a thin-film electrolyte-based battery. Reproduced with permission [60]. Copyright 2014, Elsevier. (f) Schematic illustration of mass/charge-transfer processes at an electrode/electrolyte (thin-film) interface. Reproduced with permission [22]. Copyright 2021, American Chemical Society.

NpF salt at high concentrations (> 2.2 M) without reacting with F^- (Fig. 5a). Electrolytes composed of *N,N,N*-trimethyl-*N*-neopentylammonium fluoride (Np_1F) and N,N,N-dimethyl-*N,N*-dineopentylammonium fluoride (Np_2F) in BTFE solvent were designed, respectively, demonstrating high ionic conductivity comparable with values obtained in traditional LIB electrolytes (10^{-3} to 10^{-2} S cm^{-1}; Fig. 5b). By pairing 1 M Np_1F-BTFE electrolyte with a Cu@LaF_3 composite cathode, reversible fluorination and defluorination reactions in a FIB were achieved at RT. However, poor cycling stability was displayed, attributed to the insufficient ESW of this liquid electrolyte. Following this groundbreaking work, the authors continued exploring liquid FIB electrolytes by studying ion-solvent properties. They demonstrated that various organic solvents were capable of dissolving Np_1F salt that can stabilize F^- in solution, including propionitrile (PN), 2,6-difluoropyridine (2,6-DFP), and BTFE, among which 2,6-DFP solvent enabled the highest F^- ion mobility (Fig. 5c), while BTFE solubilized a larger amount of Np_1F. In addition, the electrolyte ionic conductivity was improved via mixing amide into BTFE as a co-solvent (Fig. 5d), which was attributed to the ability of BTFE/co-solvent mixtures to promote ion dissociation between Np_1^+ cations and F^- anions [57].

To mitigate β-hydrogen elimination and/or other nucleophilic fluoride attacks towards atoms like α-H, C═O, ChN, P, Si, etc. under acidic conditions, Lewis acidic solvating agents (i.e., anion acceptors: AAs) such as organic compounds containing electropositive elements (e.g., B, Si, P, etc.) can be employed to enhance the solvation of F^- [10,71]. Ogumi et al. demonstrated that a variety of boron-containing compounds, such as fluorobis(2,4,6-trimethylphenyl) borane (FBTMPhB), triphenylboroxine (TPhBX), and triphenylborane (TPhB) could be employed as AAs in FIB electrolytes. With the aid of 0.5 M FBTMPhB as an AA, a stable electrolyte consisting of 0.45 M CsF in tetraglyme solvent was formed, achieving a high anti-oxidative voltage of ~3.6 V vs. Li/Li^+. Unfortunately, the authors found this AA also contributed to the dissolution of the active material upon charging, which caused capacity fading during subsequent cycles [72]. Afterwards, the authors demonstrated that both the type of AA and the salt concentration of CsF in the electrolytes had significant effects on the electrochemical performance of PbF_2 electrodes.

To solve the above issues of active materials' dissolution in these electrolytes, the extensively studied lithium bis(oxalato)borate (LiBOB), which is effective in suppressing cathode material dissolution in LIBs, has been considered a promising candidate for FIBs. For the first time, using tetraglyme (G4) electrolytes containing CsF and different amounts of LiBOB, Kucuk et al. investigated the effects of LiBOB on the solubility of fluorine-based salts and found the optimum BOB^- concentration and formulation to be $LiBOB_{0.25}/CsF/G4$ [73]. Following this effort, they found the addition of BOB^- not only suppressed cathode material dissolution [73–78] but also enhanced the electrochemical stability of the LiBOB-containing electrolytes compared with AA/G4 systems (e.g., via the interactions between BOB^- and Cs^+, and between fluoride and the CH_2 groups of G4) [74,76]. This design enabled the successful operation of FIBs. In this pursuit, exploring and regulating liquid electrolytes with the appropriate AA type and fluoride salt/AA ratio should be done to achieve high-performance FIBs. When designing an F-containing electrolyte, one should keep in mind that ultimately, the

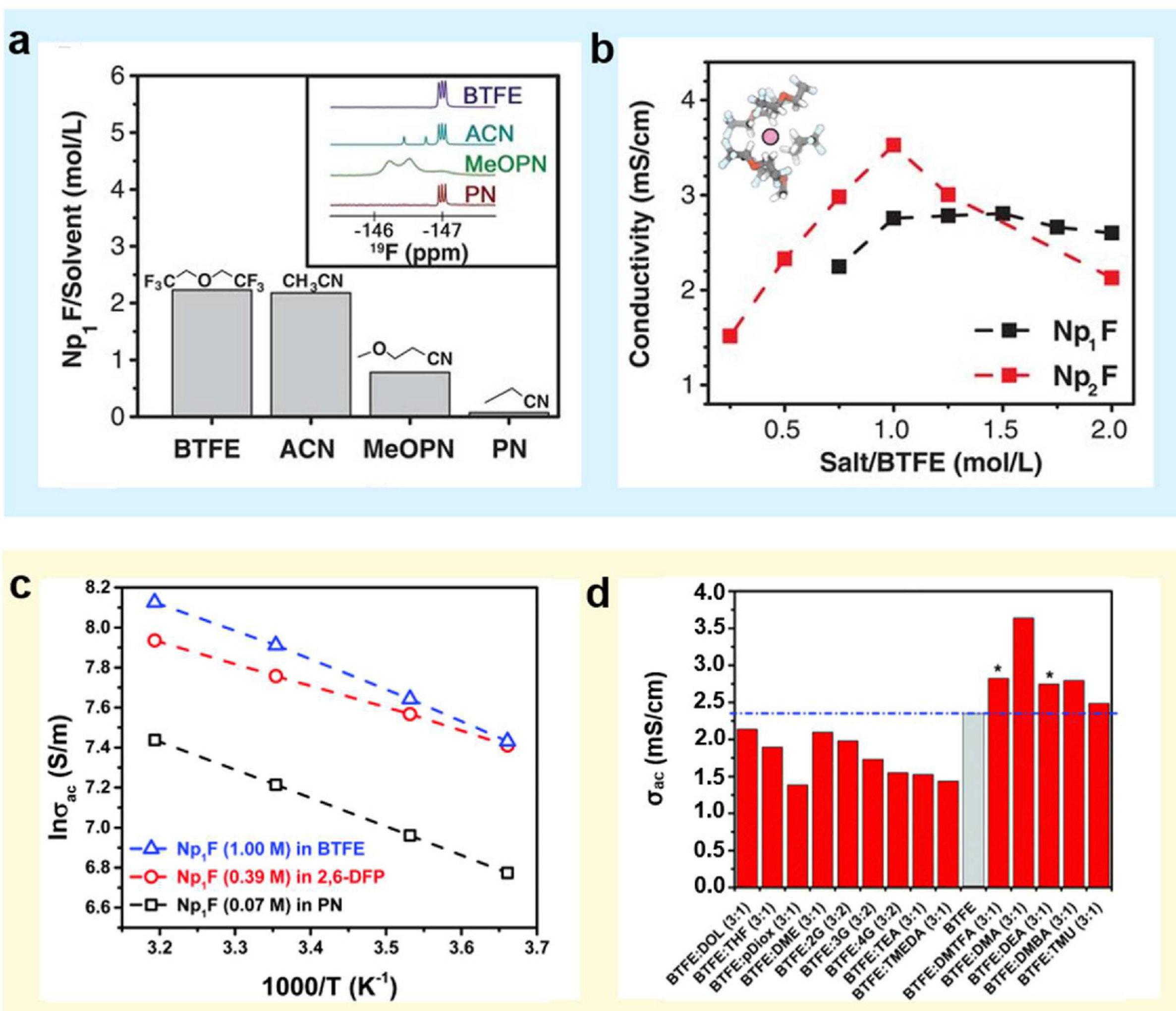

Fig. 5. Non-aqueous electrolyte for FIBs. (a) $N_{p1}F$ solubility in BTFE, acetonitrile (can), 3-methoxypropionitrile (MeOPN), and PN. Inset shows ^{19}F NMR spectra in the bifluoride region for $N_{p1}F$ dissolved in each solvent. (b) Ionic conductivity of $N_{p1}F$ and $N_{p2}F$ in liquid BTFE solutions as a function of concentration. Inset shows the simulated solvation shell of BTFE molecules surrounding F^- (pink sphere). Reproduced with permission [26]. Copyright 2018, American Association for the Advancement of Science. (c) Ionic conductivity of $N_{p1}F$ in PN, 2,6-DFP, and BTFE solvents. (d) Ionic conductivity of $N_{p1}F$ (0.75 M) in BTFE:co-solvent mixtures. Reproduced with permission [57]. Copyright 2019, Royal Society of Chemistry.

conduction and reactivity of F^- will be suppressed when F^- ion solvation is enhanced [10].

2.2.3. Aqueous electrolytes

Aqueous solutions have also been considered for designing liquid electrolytes for rechargeable FIBs. Recently, an aqueous NaF salt solution acting as the electrolyte for FIBs was proposed by Chen et al., where 4-hydroxy-2,2,6,6-tetramethyl-piperidinooxy (TEMPO) and BiF_3 were used as the cathode and anode, respectively [27]. To ensure only F^- were transported upon cell cycling, an anion exchange membrane was employed to prevent side effects due to insoluble compounds from both electrodes. After 85 cycles, the cell displayed a reversible and stable discharge capacity of 89.5 mAh g^{-1} based on the BiF_3 weight at a current density of 1000 mA g^{-1}. However, the voltage hysteresis was relatively large (~1.0 V), especially when compared with those obtained with traditional LIBs. Moreover, the formation of HF or bifluoride in the aqueous electrolyte was not discussed. For the implementation of FIBs with high capacity and environmental friendliness, other salts besides NaF need to be developed, and electrode materials compatible with aqueous electrolytes should be explored.

Above all, it should be noted that the safety issue is probably the greatest concern facing liquid F^--conducting electrolytes. These electrolytes are generally corrosive and toxic towards cell components due to the highly reactive F^-. They are also potentially more flammable than solid electrolytes, which require tuning of the electrolyte chemistry to allow practical FIBs with high safety [10]. For further detailed and specific discussion on developments in FIB electrode materials and electrolytes, readers are strongly encouraged to see Nowroozi et al.'s and Yu et al.'s excellent reviews [31,53].

3. Electrolytes for DIBs and RDIBs

By involving anions and cations simultaneously for charge transfer, unique operating mechanism for DIBs and RDIBs are achieved. Serving as a reservoir for active ions (both cations and anions), the electrolyte plays a decisive role in the cell performance of DIBs and RDIBs — e.g., the voltage of DIBs and RDIBs relies heavily on the active ions, solvent, and electrolyte concentration — while the voltage of ARBs is determined by the Gibbs free energy [79,80]. Obviously, the electrolyte design principles and related research directions for these kinds of batteries are distinctly different from those of CRBs (e.g., LIBs). This section will systematically discuss various types of electrolyte systems utilized, and their impacts on the electrochemical properties of DIBs and RDIBs.

3.1. Dual-ion batteries (DIBs)

Typically, the anion insertion/extraction at the cathode endows DIBs with a high working voltage, which is beneficial for enhancing energy/power characteristics. However, the oxidation stability of conventional organic electrolytes cannot meet the high voltage requirements for anion reaction, resulting in low Coulombic efficiency and short lifetimes for DIBs. The following section will review recent progress in electrolytes for DIBs and RDIBs, including non-aqueous (e.g., conventional organic electrolytes, fluorinated electrolytes, HCEs, ILs, and gel polymer electrolytes) and aqueous electrolytes, focusing on their ESWs and compatibility with the anion intercalation process.

3.1.1. Non-aqueous liquid electrolytes

The solvent is a vital component in an electrolyte and affects the anion insertion behaviors at the cathode. Owing to their low cost, high ionic conductivity, high dielectric constant, low viscosity, and suitable ESW, carbonates — including EC, PC, ethyl methyl carbonate (EMC), DMC, and dimethyl carbonate (DEC) — are the most extensively used organic solvents in DIBs [15,81–83]. Wang et al. revealed that the kinetics for the PF_6^- intercalation reaction was promoted with EMC solvent more than with PC, EC, or sulfone (SL) solvent, which can be ascribed to EMC's stronger affinity for PF_6^- (presumably, EMC forms stronger H···F hydrogen bonds, where H comes from the solvent and F^- is provided by PF_6^-) [84–86]. Nevertheless, such promotion of the anion insertion process by EMC solvent was not obtained when PF_6^- was replaced with other anions. The authors further revealed that the Li^+-BF_4^- ionic bonding was too tight to be split by EMC, which possessed low permittivity (dielectric constant: ~2.96), kinetically retarding the insertion process of BF_4^- into graphite cathodes. To liberate BF_4^- from Li^+, a co-solvent with high permittivity (e.g., PC, SL) to bond with Li^+, or another salt containing a larger cation, such as tetrafluoroborate ($TBABF_4$; the van der Waals radius of TBA^+ is 4.15 Å, compared with 0.76 Å for Li^+) were employed, achieving a much higher anion intercalation capacity [87,88].

Unfortunately, the high voltage required for the anion intercalation process exceeds the oxidation stability voltage of conventional carbonates, hindering the development of high-voltage electrolyte systems. Ascribed to the decreased HOMO energy level, solvent molecules containing the sulfonyl group (-S(=O)$_2$-) were demonstrated to enhance the electrolyte oxidation stability to ~6 V (vs. Li/Li^+) [89]. An electrolyte composed of 2 M $LiPF_6$ salt in ethyl methyl sulfone (EMS) solvent allowed a graphite||Li DIB to work within 3.5–5.45 V with a high capacity of 95 mAh g^{-1} [90]. Phosphates have also proven effective in achieving high-voltage electrolytes, owing to their ability to form protective CEI films and their nonflammability [91]. As a strong electron-donating solvent, trimethyl phosphate (TMP) was used by Cui et al. to reconfigure the anion solvation structure, yielding a 1.5 M $Zn(TFSI)_2$-EMC/TMP (1:3 by volume) electrolyte. Thereby, the $TFSI^-$ anions were confined in the solvation regime of TMP, liberating the EMC solvent from the EMC-$TFSI^-$ complex into a free state (Figs. 6a and b), which elevated the oxidation voltage of carbonate electrolytes to 3 V vs. Zn/Zn^{2+}. The resulting graphite||Zn DIB achieved a capacity retention of 92% over 1000 cycles [92]. By introducing electron-withdrawing fluorine, fluorinated solvents with lower HOMO energy contributed to enhanced anti-oxidation stability.

Fluorinated solvents have also proven effective in forming a stable SEI layer on the anode and/or CEI layer on the cathode [93]. The first fluorinated electrolyte employed in DIBs was reported by Read et al., consisting of 1.7 M $LiPF_6$ in fluoroethylene carbonate (FEC)/EMC with 5 mM tris(hexafluoro-isopropyl) phosphate (HFIP) as an additive. This electrolyte was demonstrated to support the reversible charging/discharging process of a 5.2 V graphite||graphite battery with a lifetime of 50 cycles [94]. Recently, Yang et al. proposed that FEC co-solvent participated in the solvation structures of Na^+ cations and PF_6^- anions via replacing the original EMC solvent, constructing both a fluorinated CEI film on graphite cathodes and a NaF-rich SEI layer on Na metal anodes. Based on a modified 1 M $NaPF_6$-EC/DMC/EMC (1:1:1 by volume) electrolyte containing 10 wt% FEC additive, graphite cathodes with long cyclability and high reversibility were achieved [23]. Notably, owing to their high anti-oxidation ability (stable over 6 V vs. Li/Li^+), nitriles have been considered as potential high-voltage electrolytes in LIBs [95], yet no related work with DIBs has been reported.

Owing to their broad ESW, excellent thermal stability, nonflammability, and low volatility, ILs — specifically room-temperature-molten salts-based electrolytes — have emerged as a strategy to enable outstanding stability/reversibility in high-voltage DIBs [98,99]. However, the major challenge facing these IL-based electrolytes is their inability to form an effective SEI film on anode materials (e.g., graphite anode), leading to the co-intercalation of large IL cations (e.g., 1-butyl-1--methylpyrrolidinium cations; Py_{14}^+) along with Li^+ insertion (Pyr_{14}TFSI-LiTFSI electrolyte system) [100]. Additives such as vinylene carbonate and vinyl ethylene carbonate have been reported to suppress solvent co-intercalation by forming effective SEI layers [101,102]. In another effort, pure IL (PP_{14}TFSI) was employed to supply ionic charge carriers, where $TFSI^-$ and PP_{14}^+ were successfully intercalated into a graphite cathode and graphite anode simultaneously upon charging. Within the voltage range of 1.0–5.0 V, a discharge capacity of 82 mAh g^{-1} was obtained without obvious capacity decay over 600 cycles. In addition, the

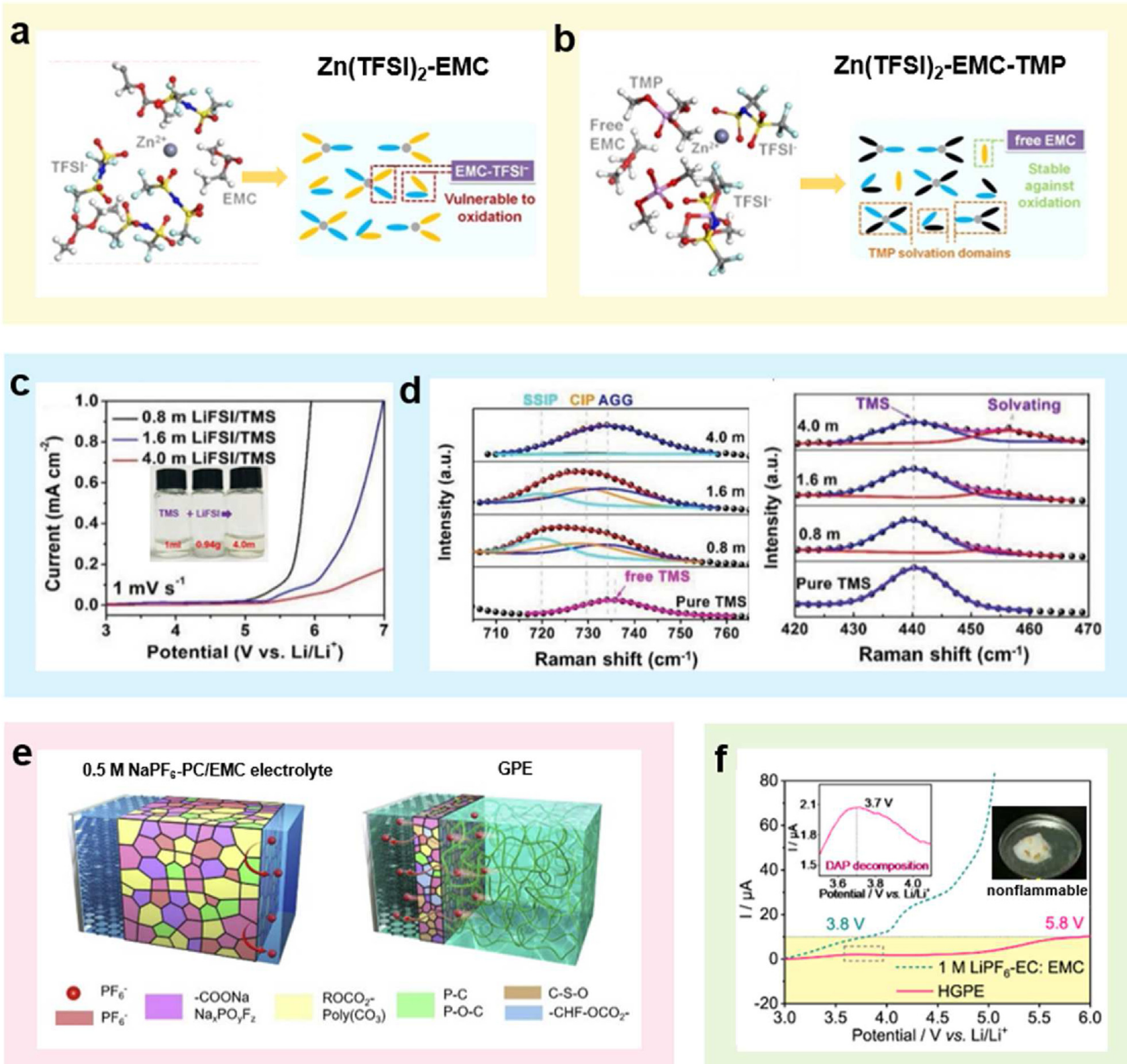

Fig. 6. Non-aqueous electrolytes for DIBs. Representative solvation structures for (a) 1.5 M Zn(TFSI)$_2$-EMC and (b) 1.5 M Zn(TFSI)$_2$-EMC/TMP electrolyte for graphite||Zn DIB. Reproduced with permission [92]. Copyright 2020, Wiley-VCH. (c) LSV results under different electrolyte concentrations. (d) Raman results for LiFSI-TMS electrolytes. Reproduced with permission [96]. Copyright 2021, Wiley-VCH. (e) Schematic illustrations of the CEI compositions on graphite cathodes using 0.5 M NaPF$_6$-PC/EMC electrolyte and GPE, respectively. Reproduced with permission [24]. Copyright 2020, Elsevier. (f) LSV curves of 1 M LiPF$_6$-EC/EMC electrolyte and GPE at a scan rate of 5 mV s^{-1} (inset shows the nonflammability of the GPE). Reproduced with permission [97]. Copyright 2020, Springer.

appropriate viscosity and conductivity of the PP$_{14}$TFSI electrolyte enabled a reduced self-discharge rate compared with other pure ILs [103]. Overall, current IL systems require further exploration to enhance the compatibility of both the cathode and the anode, as well as reduce the viscosity and improve the ionic conductivity.

In recent years, HCEs have been recognized as a new electrolyte design strategy to reinforce the interactions between cations and anions/solvent molecules and also reduce the fraction of free solvent molecules [104]. HCEs display peculiar physicochemical and electrochemical properties in comparison to conventional dilute electrolytes: with fewer free solvents, HCEs are expected to achieve higher oxidation stability; in addition, enhanced solvent–cation interaction can decrease solvent volatility, thus endowing the battery with a high level of safety [104]. Since active ions are supplied solely by the electrolyte salts, employing HCEs is beneficial to decrease the usage of electrolyte solvent, thus enhancing the energy density of DIBs. Kravchyk et al. presented a graphite||K DIB that utilized an HCE of 5 M potassium bis(fluorosulfonyl) imide (KFSI)-EC/DMC, achieving an energy density of up to 207 Wh kg^{-1} (calculated based on the mass of electrolyte and the active materials of both electrodes) with an average discharge voltage of 4.7 V [105]. Recently, Tang et al. developed an HCE consisting of 4 M lithium bis(-fluorosulfonyl)imide (LiFSI) in tetramethylene sulfone (TMS). Owing to the disappearance of free TMS solvent in this HCE, excellent anti-oxidative stability of up to ~6.0 V vs. Li/Li$^+$ was achieved (Figs. 6c and d), contributing to significantly suppressed detrimental gas formation and thus a reversible de-/insertion process for FSI$^-$ at the graphite cathode under a high working voltage. The resulting graphite||Li DIB delivered a reversible capacity of 113.3 mAh g^{-1} with a medium voltage of ~4.6 V, based on the active mass of the cathode, along with 94.7% retention after 1000 cycles [96]. Although their wide ESWs can satisfy the high working voltage required for anion insertion, HCEs still face major challenges, such as high viscosity, high cost, and poor wettability towards both the separator and the electrodes.

In light of their high safety (e.g., avoiding liquid leakage), high ionic conductivity, excellent electrochemical stability, and good flexibility, gel polymer electrolytes (GPEs) have also been explored in DIBs. In 2018, Tang et al. developed the first GPE based on the poly(vinylidene fluoride-hexafluoro propylene) (PVDF-HFP) polymer, which was co-doped with PEO and graphene oxide (GO) via weak bond interactions. The GO was favorable for improving the mechanical property and thermal stability, while the PEO optimized the pore configuration of the GPE. After soaking in a liquid electrolyte (4 M $LiPF_6$-EMC with 2% vinylene carbonate (VC) additive), this modified GPE with a 3D porous network greatly increased the ionic conductivity to 2.1 mS cm^{-1}, contributing to excellent rate capability and cycling stability (92% capacity retention after 2000 cycles) at 5 C for graphite||Al DIBs [106]. Later in 2020, Tang and coworkers further demonstrated that a GPE consisting of PVDF-HFP crosslinked by Al_2O_3 nanoparticles via Lewis acid–base intermolecular bonding is also promising for realizing high-performance flexible DIBs [107].

Multifunctional GPEs prepared by in situ thermal-induced polymerization were previously reported by our group [24]. In one work, ethoxylated pentaerythritol tetraacrylate (EPTA) monomer was polymerized in situ in an optimized electrolyte of 0.5 M $NaPF_6$-PC/EMC/FEC (1:1:1 by volume) with 1,3-pro-panesultone (PS) as an additive to obtain a GPE [24]. The FEC co-solvent and PS additive significantly enhanced the anti-oxidative stability of the electrolyte (up to 5.5 V vs. Na/Na^+), constructed stable CEI/SEI layers on both electrodes, and enabled highly efficient intercalation/plating of anions and cations. The as-designed GPE also displayed a high ionic conductivity (5.33 mS cm^{-1}) and high safety. As a result, a graphite||Na DIB (Fig. 6e) achieved an energy density of up to 484 Wh kg^{-1} at a working voltage of 4.4 V based on the graphite mass, as well as superior long-term cycling stability. Following this work, our group developed a new GPE prepared from in situ copolymerization of diethyl allyl phosphate (DAP) monomer and pentaerythritol tetraacrylate (PETEA) crosslinker in an all-fluorinated electrolyte. This GPE demonstrated similar advantages (Fig. 6f), such as high safety (i.e., nonflammability and non-leakage), high ionic conductivity, and a high anti-oxidative voltage of up to 5.5 V vs. Li/Li^+. It is very interesting to note that residual DAP after polymerization acted as a CEI-forming additive to suppress solvent co-intercalation and other side reactions between the GPE and the graphite cathode. Consequently, a highly reversible de-/intercalation process of $PF_6{}^-$ anions from/into graphite cathodes was enabled [97]. These reports demonstrate the great potential of GPEs for realizing high-performance DIBs, and more interesting work can be expected in the future.

3.1.2. Aqueous electrolytes

Organic liquids may give rise to concerns about cost, eco-friendliness, and safety, severely restricting the large-scale applications of DIBs. To tackle these issues, aqueous or hybrid aqueous/nonaqueous electrolytes (Table 2) have emerged as highly interesting candidates for developing novel DIBs [25,108–110]. Employing a simple aqueous NH_4NO_3 electrolyte (1 M), Ji et al. demonstrated reversible intercalation/de-intercalation into/from Mn_3O_4 cathode for the first aqueous DIBs. Electrochemical quartz crystal microbalance (EQCM) tests revealed that around two H_2O molecules were co-intercalated into Mn_3O_4, accompanied by one $NO_3{}^-$ insertion. The as-prepared Mn_3O_4||activated carbon (AC) DIB delivered a discharge capacity as high as 183 mAh g^{-1} at 0.1 A g^{-1}, based on the active mass of the cathode, which is one of the highest reversible capacities achieved by state-of-the-art graphite cathode-based DIBs. This cell also demonstrated fast reaction kinetics for $NO_3{}^-$ in the Mn_3O_4 structure [110]. Later on, another work based on 1 M $(NH_4)_2SO_4$ aqueous electrolyte was reported by Zhang and co-workers, who presented a novel DIB consisting of an n-type polyimide (PI) anode for the $NH_4{}^+$ reaction and a p-type radical polymer cathode (PTMA) for the $SO_4{}^{2-}$ reaction during battery operation. This as-assembled battery enabled a high working voltage of 1.9 V and an excellent cycle life of 10,000 cycles with 86.4% capacity retention at 5 A g^{-1}, as well as a maximum energy density of 51.3 Wh kg^{-1} and a maximum power density of 15.8 kW kg^{-1} (based on the total weight of the cathode and anode materials) [25]. These reports provide new insights into designing novel aqueous DIBs; nevertheless, the narrow stability window limits the working voltage and energy output of aqueous DIBs.

Recently, a new class of "water-in-salt" (WiS) electrolytes formulated with superconcentrated lithium salts (> 21 m, mol kg^{-1}) has been developed by Xu and co-workers, significantly enlarging the stability window of aqueous electrolytes from 1.23 to ~4.9 V [108,122]. With regard to relatively dilute electrolytes (≤ 5 m), hydrated Li^+ remains in its primary solvation sheath in the presence of free H_2O molecules, whereas the activity of H_2O molecules is significantly suppressed in a WiS electrolyte, as nearly all H_2O molecules participate in forming the ion solvation shells (Fig. 7a). A WiS electrolyte of 20 m NaFSI + 0.5 m $Zn(TFSI)_2$ was explored in a graphite||Zn DIB by Placke et al., where Zn^{2+} and $TFSI^-$ functioned as the predominant intercalants, while a 20 m NaFSI concentration effectively reduced the free water amount in the WiS electrolyte (Fig. 7b) [19]. The WiS electrolyte provided enhanced anodic stability, from ~1.4 V for the dilute electrolyte (1 m NaFSI + 0.5 m $Zn(TFSI)_2$) to ~1.8 V vs. Ag|AgCl, enabling anion storage during the electrochemical oxidation of the graphite cathode (Fig. 7c). As a consequence, the as-assembled graphite||Zn DIB displayed a reversible capacity of ~110 mAh g^{-1} at 200 mA g^{-1}, which retained > 80% capacity over 200 cycles. Benefiting from the high average discharge voltage of ~2.25 V, an energy density of ~200 Wh kg^{-1} was achieved based on the active material of the cathode.

More interestingly, WiS electrolytes also promote highly efficient halogen conversion–intercalation chemistry at graphite cathodes. According to the work by Wang et al., the sequential intercalation of Br^- and Cl^- (Figs. 7b and c) was realized by developing a composite cathode consisting of $(LiBr)_{0.5}(LiCl)_{0.5}C_{\sim 3.7}$ (LBC-G). A hydrated LiBr/LiCl layer ($LiBr\cdot 0.34H_2O$–$LiCl\cdot 0.34H_2O$) was formed via extracting water from a WiS electrolyte (21 m LiTFSI + 7 m lithium trifluoromethanesulfonate (LiOTf) in water), separating the LBC-G surface from the electrolyte, and regulating the dynamic water equilibrium. During charging, Br^- within the hydration layer was oxidized to Br^0 first, then intercalated into graphite via one-electron transfer. When the charging continued, the oxidation and intercalation of Cl^- occurred (one-electron transfer), forming a mixed intercalation compound (Figs. 7d and e). The Cl^0 and Br^0 were extracted from the graphite material to form solid LiCl/LiBr upon discharging. It was demonstrated that a stage-1 graphite intercalation compound (GIC) was formed, contributing to a high reversible capacity of 243 mAh g^{-1} based on the total weight of the electrode. When paired with a highly fluorinated ether (HFE)/PEO-protected graphite anode, a 4 V-class full cell enabled full reversibility with ~100% CE, along with a high energy density of 460 Wh kg^{-1}, based on the total mass of the cathode and anode [111]. Inspired by this work, Ji et al. demonstrated reversible storage of I–Cl interhalogen ($[ICl_2]^-$) at a graphite cathode by employing an aqueous deep eutectic solvent (DES) gel electrolyte of 120 m choline chloride (ChCl) + 30 m $ZnCl_2$ + 5 m KI. As a consequence, the graphite cathode delivered a high reversible capacity of 291 mAh g^{-1} at 30 mA g^{-1}, based on the mass of the cathode material, with stable cycling performance [118]. Overall, these findings reveal that the WiS strategy not only widens the ESWs of aqueous electrolytes but also facilitates the intercalation/de-intercalation process of anions into/from cathode materials.

Hybrid aqueous/nonaqueous electrolytes have also been explored to achieve both high safety from nonflammable aqueous WiS electrolytes and broad ESWs via non-aqueous solvents. Combining 21 M LiTFSI-H_2O with 9.25 M LiTFSI-DMC in a mass ratio of 1:1, Placke et al. demonstrated a stage-2 GIC of the $TFSI^-$ intercalation reaction with a graphite cathode. When coupled with lithium titanium phosphate ($LiTi_2(PO_4)_3$; LTP) material as the anode, the full battery exhibited a reversible capacity of ~42 mAh g^{-1}, based on the active mass of the cathode, as well as 71% capacity

Table 2
Electrochemical performance of typical aqueous electrolytes for DIBs and RDIBs.

Electrolyte	Cathode||Anode	Output voltage (V)	Specific capacity (mAh g^{-1})	Retained capacity (mAh g^{-1})/cycles	Ref.
1 M NH_4NO_3	Mn_3O_4||AC	0.0–1.0 (vs. Ag|AgCl)	~150 at 1 A g^{-1}	50/3500	[110]
1 M $(NH_4)_2SO_4$	PTMA||PI	0.0–1.9	~100 at 5 A g^{-1}	~86.4/10,000	[25]
20 m NaFSI + 0.5 m $Zn(TFSI)_2$	Graphite||Zn	0.2–2.7	110 at 80 mA g^{-1}	~88/200	[19]
21 m LiTFSI + 7 m LiOTf	LBC-G||Graphite	3.4–4.5	127 at 3 mA g^{-1}	94/150	[111]
8 m $Zn(ClO_4)_2$	Graphite||Zn	0.5–2.5	45 at 100 mA g^{-1}	~23.5/500	[112]
21 M KFSI	PTPAn||PTCDI	0.0–1.6	47 at 500 mA g^{-1}	~25/900	[113]
2 M $NaClO_4$	NNH||NTP@C	0.2–1.5	~76 at 1.33 A g^{-1}(-20 °C)	~64.6/10,000	[114]
1 m $Zn(OTf)_2$ + 19 m LiTFSI	BDB||Zn	0.4–2.1	112 at 390 mA g^{-1}	~91.8/500	[115]
30 m $ZnCl_2$	NFG||Zn	0.8–1.95	134 at 100 mA g^{-1}	82/800	[116]
33.3 m LiFSI + 3.7 m LiTFSI	Graphite||AC	0.0–3.2	72 at 100 mA g^{-1}	~70/100	[117]
120 m choline chloride + 30 m $ZnCl_2$ + 5 m KI	Graphite||Zn	−0.2-1.4 (vs. Ag|AgCl)	291 at 30 mA g^{-1}	260/40	[118]
30 m $ZnCl_2$	Polypyrene||Zn	0.6–1.8	180 at 50 mA g^{-1}	175.3/800	[119]
5 m $MgCl_2$ + 5 m TBMACl	Graphite||PTCDI	0.0–2.18	41 at 50 mA g^{-1}	33/200	[120]
1 M KF	Prussian blue|| BFO	0.0–2.0	153.7 at 1 A g^{-1}	~61.5/1000	[18]
0.8 M NaF	$Na_{0.44}MnO_2$||BiF_3	0.0–1.5	123 at 100 mA g^{-1}	47.28/40	[121]
30 m $ZnCl_2$	$Zn_3[Fe(CN)_6]_2$|| ferrocene/AC	0.0–1.6	25 at 150 mA g^{-1}	14.5/1000	[13]

Note: (PTMA); (PI); activated carbon (AC); $(LiBr)_{0.5}(LiCl)_{0.5}C_{\sim3.7}$ (LBC-G); polytriphenylamine (PTPAn); 3,4,9,10-perylenetetracarboxylic diimide (PTCDI); nano/microstructured $Ni(OH)_2$ (NNH); carbon-coated $NaTi_2(PO_4)_3$ (NTP@C); 1,4 bis(diphenylamino)-benzene (BDB); nitrogen-doped few-layered graphene (NFG); tributylmethylammonium chloride (TBMACl); BiF_3@$Bi_7F_{11}O_5$@reduced graphene oxide (BFO).

retention after 500 cycles at 200 mA g^{-1}. The low average discharge voltage of 1.5 V was unsatisfactory but could be further enhanced to 2.5 V by substituting the LTP with a LTO anode [109]. Following this work, Yan et al. designed another hybrid electrolyte by mixing a WiS electrolyte (7 m LiOTF and 21 m LiTFSI dissolved in water) with a non-aqueous electrolyte of 9.25 m LiTFSI in DMC. Despite the high salt concentration, the hybrid electrolyte achieved an ionic conductivity of 0.65 mS cm^{-1} at 25 °C, providing good wettability towards the cathode and anode materials. A full DIB based on the hybrid electrolyte was constructed, with graphite as cathode and niobium pentoxide (Nb_2O_5) as anode, delivering a reversible capacity of 47.6 mAh g^{-1} at a current density of 200 mA g^{-1}, based on the cathode material, a medium voltage of up to ~2.2 V, and a high CE of 93.9% [108].

3.2. Reverse dual-ion batteries (RDIBs)

RDIBs follow a similar operating mechanism as DIBs, but the sequence of the anion- and cation-storage chemistries is flipped. In addition, the incorporation of both types of ions into the electrodes occurs during the discharging process, which is opposite to what occurs upon charging in DIBs.

Up till now, only aqueous electrolytes have been reported to support RDIB chemistries. The concept of the RDIB was defined by Ji et al. for the first time, employing a 30 m $ZnCl_2$ WiS electrolyte that supplied $ZnCl_4^{2-}$ anions and Zn^{2+} cations for charge storage. Combined with a Zn-insertion Prussian blue ($Zn_3[Fe(CN)_6]_2$) cathode and a ferrocene/activated carbon nanocomposite (Fc/C) anode, this electrolyte enabled the RDIB to proceed by an initial discharge process via the insertion of $ZnCl_4^{2-}$ and Zn^{2+} into the anode and cathode, respectively. During charging, both cations and anions were released back to the electrolyte (Fig. 8a). Notably, the electrolyte also served as the sole reservoir of ionic charge carriers (anions and cations) for energy storage, thus being regarded as the active material in RDIBs [13]. Benefiting from the unique nature of a WiS electrolyte with few free water molecules, the dissolution issue of the ferrocene material was mitigated. Furthermore, the voltage for cation insertion was raised while the voltage related to anion insertion was reduced, thereby enlarging the $Zn_3[Fe(CN)_6]_2$||Fc/C battery voltage by 0.35 V compared with one using a dilute electrolyte containing 5 m $ZnCl_2$ (Fig. 8b). Consequently, a reversible capacity of ~30 mAh g^{-1} was achieved, based on the active masses of both electrodes [13].

In 2018, a rechargeable RDIB based on F^- anion and Na^+ cation electrochemistry was proposed by Hou and co-workers, comprising 0.8 M NaF aqueous electrolyte, $Na_{0.44}MnO_2$ cathode, and BiF_3 anode. During the initial charging process, F^- and Na^+ were released from the anode and cathode materials, respectively, to the electrolyte, while the two types of ions were captured by the corresponding electrodes in the following discharge period. This battery exhibited a high discharge capacity of ~123 mAh g^{-1} at 100 mA g^{-1}, based on the mass of the BiF_3 material, but the capacity decayed rapidly to 47.28 mAh g^{-1} within 40 cycles [121]. Very recently, utilizing KF aqueous solution as the electrolyte, Li et al. constructed a fluorine/potassium RDIB based on Prussian blue (PB) as the cathode material and BiF_3@$Bi_7F_{11}O_5$@reduced graphene oxide (BFO) as the anode material. It was revealed that although the capacity decreased with lower electrolyte concentration (1–12 M), the cycling stability was improved due to less dissolution of BiF_3 and fewer undesirable surface deposits. In addition, the rational design of the anode with added $Bi_7F_{11}O_5$ and a graphene coating contributed to reduced volume change, enhanced electronic conductivity, and suppressed pulverization. Therefore, with 1 M KF electrolyte, a high discharge capacity of 218 mAh g^{-1} at 1 A g^{-1}, based on the mass of the anode material, and excellent rate performance with 47% retention maintained at 5 A g^{-1} were achieved (Figs. 8c and d) [18].

4. Conclusions and perspective

As an emerging new type of battery chemistry, ASBs (i.e., ARBs, DIBs, and RDIBs) utilizing anions as charge carriers for storage reactions have received growing interest and exhibited great potential for grid-scale energy storage. As an essential and indispensable component, ASB electrolytes should comply with the same key requirements as LIBs, including high ionic conductivity, good chemical stability/inertness, wide ESW, low interfacial resistance, etc., thus enhancing the kinetics/reversibility of electrochemical reactions in ASBs. In this review, we have summarized the research progress and recent achievements in electrolytes for ARBs, DIBs, and RDIBs, including solid electrolytes, non-aqueous liquid electrolytes, and aqueous electrolytes. We have mainly focused on discussing the unique properties and basic principles for designing each type of electrolyte, as well as various performance parameters, such as working voltage, lifetime, energy/power density, safety, cost, etc. The properties of different types of electrolytes in ARBs and DIBs/RDIBs were compared in terms of the six aspects depicted in Fig. 9. It is clear that except for high ionic conductivity, these aspects are far from satisfactory in aqueous electrolytes for ARB applications. In addition, although solid electrolytes display high resistance for ionic

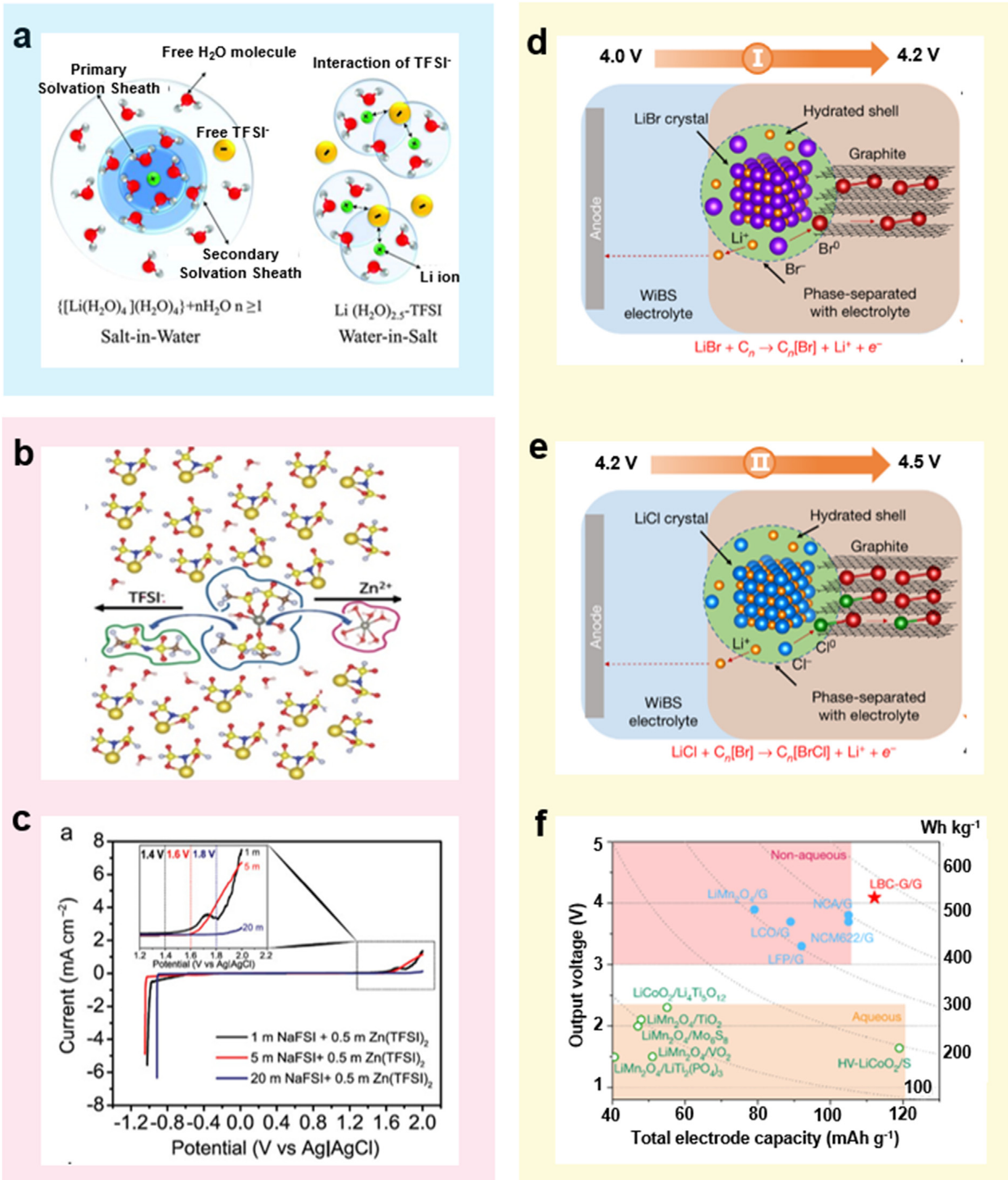

Fig. 7. Aqueous electrolytes in DIBs. (a) Illustration of the Li^+ primary solvation sheath in dilute and WiS electrolytes. Reproduced with permission [122]. Copyright 2015, American Association for the Advancement of Science. (b) Simulated cation solvation structure in 20 m NaFSI + 0.5 m $Zn(TFSI)_2$ WiS electrolyte (based on optimized first solvation shells of Na^+ and Zn^{2+}). (c) ESWs of electrolytes measured at a scan rate of 1 mV s^{-1} in an AC||Ti cell with an Ag|AgCl reference electrode. Reproduced with permission [19]. Copyright 2020, Wiley-VCH. Schematic of the two-stage reaction for the LBC-G composite cathode in WiS aqueous-gel electrolyte during the charging process: (d) oxidation and intercalation of Br^-, (e) oxidation and intercalation of Cl^-, (f) energy density (red star) of the LBC-G||graphite full cells in comparison with state-of-the-art commercial and reported Li^+ chemistries using non-aqueous (blue color) and aqueous (green color) electrolytes. The energy densities were calculated based on the total weight of the cathode and anode. Reproduced with permission [111]. Copyright 2019, Springer.

conduction, they surpass liquid electrolytes in mechanical properties and thermal stability. With respect to electrolytes developed in DIBs/RDIBs, the electrochemical stability of aqueous electrolytes requires further improvement to broaden their applications.

Different types of ASBs have unique electrolyte requirements. With respect to DIBs and/or RDIBs, where the electrolyte serves as the reservoir supplying both cations and anions for charge transfer, the salt concentration and the corresponding physical nature of the electrolyte depend highly on the SOC in DIBs and/or RDIBs, compared with the unchanged ion concentration during charging/discharging for ARBs, where the electrolyte only acts as the charge carrier to transport anions. Thus, besides physical properties, the electrolyte formulation (e.g., the

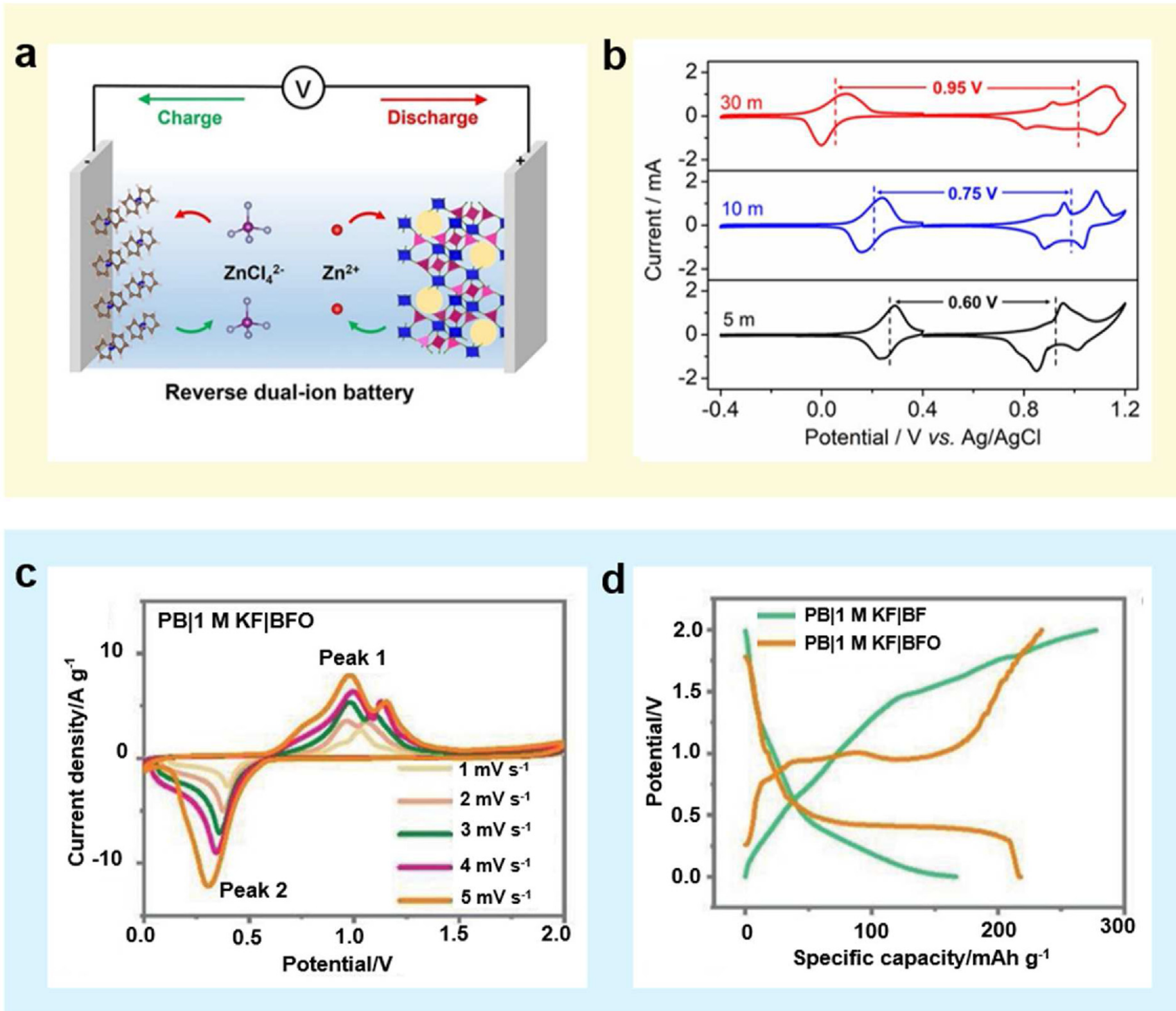

Fig. 8. Aqueous electrolytes in RDIBs. (a) Schematic of the working mechanism of a $Zn_3[Fe(CN)_6]_2$||Fc/C RDIB. (b) CV curves of the Fc/C anode and $Zn_3[Fe(CN)_6]_2$ cathode in $ZnCl_2$ electrolyte. Reproduced with permission [13], Copyright 2019, American Chemical Society. (c) CV curves at various scan rates and (d) charge/-discharge profiles of 1 A g^{-1} of PB||BFO cell with 1 M KF electrolyte. Reproduced with permission [18]. Copyright 2021, Wiley-VCH.

solvent type, salt and salt content, and additive amount) will also affect the reversible capacity, cell voltage, energy/power density, etc. of DIBs and/or RDIBs. In addition, electrolyte–electrode compatibility plays a significant role in reversible/stable storage reactions in ARBs. Generally, most CIBs/FIBs suffer from severe electrode dissolution and/or irreversible side reactions between electrode materials and liquid electrolytes, leading to fast capacity decay and short lifetime, and poor interfacial contact remains a tough challenge for CIBs/FIBs to improve the cycling stability. With regard to DIBs, especially with graphite cathodes, reversible anion de-/intercalation at high voltage can be compromised by incompatibility between the electrolyte and graphite, resulting in inevitable electrolyte decomposition, solvent co-intercalation, and low Coulombic efficiency. Although encouraging progress has been achieved in recent years, limitations and challenges remain for electrolyte development. Therefore, great efforts in electrolyte design should continue in the following directions:

(1) **ARBs**

With regard to CIBs, solid, non-aqueous liquid, and aqueous electrolytes can be developed for Cl^- conduction. The employment of solid electrolytes is a promising strategy to resolve issues related to electrode dissolution and/or side reactions between the electrolyte and the electrode. Through structural engineering, exploring inorganic chloride ion conductors (like halide perovskites) and multifunctional polymer-based solids can achieve high ionic conductivity and high structural stability at RT. In addition, synergistic effects can be obtained via immobilizing Cl^--containing ILs within polymer matrices, where the ILs act as both plasticizer and Cl^- supplier, which can be a promising solution to achieve high ionic conductivity as well as thermal and electrochemical stability [47]. With regard to aqueous electrolytes, employing other chloride salts beyond NaCl, and applying WiS or DES strategies are expected to widen the electrolyte electrochemical window and improve the compatibility/stability of electrode materials towards aqueous electrolytes. It should be noted that the onset potential for Cl_2 gas formation is 1.36 V vs. SHE, which ought to be considered when designing aqueous electrolyte systems.

Compared to the use of Cl^- as the charge carrier in CIBs, the smaller size and higher electronegativity of F^- enables faster ionic transport and higher anti-oxidation stability for FIBs. Although significant progress has been made in recent years regarding fluorite-type and tysonite-type structured solids, high operating temperature ($>$ 140 °C), low ionic conductivity, poor interfacial contact, etc. are still tough challenges, requiring further exploration and optimization of F^- solid conductors (e.g., creating more defects, utilizing the effect of lone pairs, optimizing synthesis strategies). Further, considering liquid electrolytes can achieve

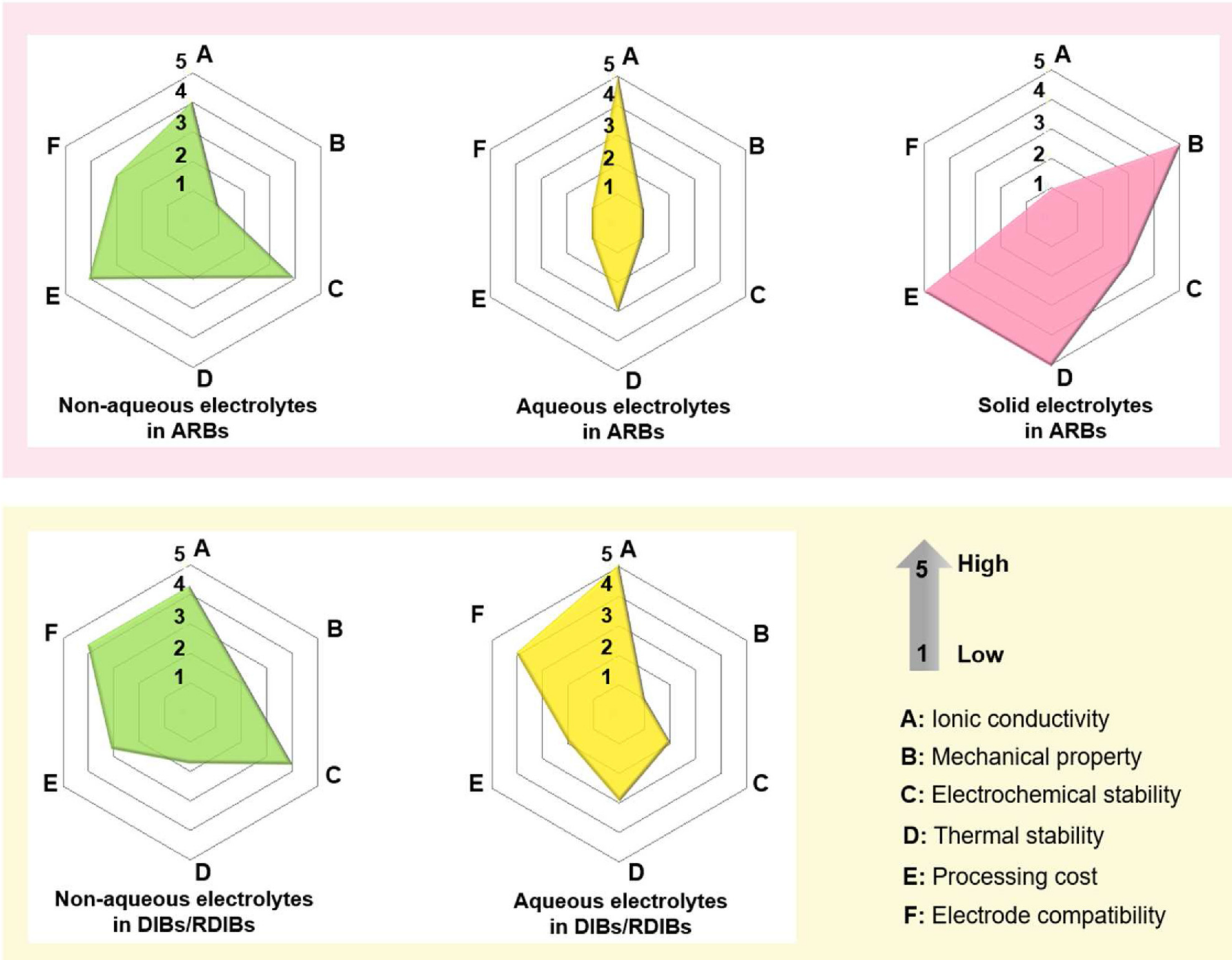

Fig. 9. Radar plots of properties for non-aqueous, aqueous, and solid electrolytes in ARBs (top), and DIBs or RDIBs (bottom).

ambient battery operation, developing stable liquid electrolytes to enable efficient FIB functioning is of vital significance, pointing toward the exploration of suitable solvents and/or fluoride salts to suppress nucleophilic F^- attack (e.g., β-hydrogen elimination) or solvating F^- by Lewis acidic agents to reduce its basicity. The safety issue is probably the greatest concern facing liquid F^--conducting electrolytes, which are potentially corrosive and toxic towards cell components due to the chemically reactive F^- ions. These electrolytes are generally flammable, requiring updating of the electrolyte chemistry to promote practical FIBs with high safety.

(2) **DIBs**

The anion intercalation process in DIBs requires a high working voltage, which relies heavily on the active ions, solvents, and electrolyte concentration. Ideally, one would design high-voltage electrolyte systems based on anti-oxidative solvents like sulfones, phosphates, fluorinated carbonates, nitriles, etc. Developing concentrated non-aqueous electrolytes, and aqueous or hybrid aqueous/nonaqueous-based WiS electrolytes are also effective strategies to facilitate the anion intercalation/de-intercalation process and enhance the energy density of DIBs. In addition, functional additives that can promote the formation of multifunctional surface layers (i.e., CEIs) on the graphite cathode should be explored further, to potentially suppress solvent co-intercalation and side reactions between the electrolyte and the cathode at high voltage. Furthermore, multivalent anions with more charge numbers and/or single halide ions (e.g., F^-, Cl^-) with smaller anionic charge carriers should be explored to potentially provide high theoretical specific capacity and energy density. To achieve high safety, high ionic conductivity, excellent electrochemical stability, and good flexibility, developing a multifunctional GPE via in situ polymerization (e.g., thermal-induced) is regarded as a feasible path for promoting high-performance DIBs.

(3) **RDIBs**

Up till now, only aqueous electrolytes have been reported for achieving RDIB chemistries, providing vast opportunities for electrolyte exploration. In addition to single halide ions (e.g., F^-, Cl^-), metal-based superhalides (e.g., based on Zn–Cl or Mg–Cl) formed in WiS- or DESs-based electrolytes may also serve as promising charge carriers [9]. As more new electrolyte systems are designed, the output voltage and the corresponding energy density of RDIBs will be expected to improve.

(4) **Microscopic mechanisms for anions as the charge carriers**

Compared with the extensive investigations of cation solvation in CRBs (e.g., LIBs), the solvation/de-solvation behavior of anions and their impacts on CEI/SEI features (e.g., chemical composition, atomic-level microstructure, mechanical property, structural evolution, interfacial resistance, ionic transport, etc.) and anion storage performance remain unclear. Therefore, theoretical calculations in combination with advanced characterization technologies (e.g., cryo-electron microscopy, in situ transmission electron microscopy (TEM), in situ X-ray photoelectron spectroscopy (XPS), and time-of-flight secondary ion mass spectrometry (TOF-SIMS)) should be conducted to investigate the microscopic mechanisms of anions as charge carriers and further manipulate the anion storage process.

Overall, the ASB technology employing anions as charge carriers for storage reactions is currently at a rather early stage, offering vast opportunities for further improvements in both fundamental and technical aspects. Significant efforts to address the above challenges and pursue these new directions will greatly enhance progress in ASB electrolyte systems, thus endowing ASBs with highly competitive features compared with state-of-the-art LIBs or other rechargeable metal-ion batteries. It is expected that with ongoing developments and enhancements in cycling stability and energy density, ASB technology will be a highly promising candidate for grid-scale energy storage at low cost.

Declaration of competing interest

The authors declare that they have no known competing financial interests or personal relationships that could have appeared to influence the work reported in this paper.

Acknowledgments

B.H. Li would like to thank the support provided by National Nature Science Foundation of China (No. 51872157 and No. 52072208) and Local Innovative and Research Teams Project of Guangdong Pearl River Talents Program (2017BT01N111).

References

[1] M.S. Whittingham, Lithium batteries and cathode materials, Chem. Rev. 104 (2004) 4271–4302.
[2] B. Dunn, H. Kamath, J.-M. Tarascon, Electrical energy storage for the grid: a battery of choices, Science 334 (2011) 928–935.
[3] R. Schmuch, R. Wagner, G. Hörpel, T. Placke, M. Winter, Performance and cost of materials for lithium-based rechargeable automotive batteries, Nat. Energy 3 (2018) 267–278.
[4] G.E. Blomgren, The development and future of lithium ion batteries, J. Electrochem. Soc. 164 (2016) A5019–A5025.
[5] P.K. Nayak, L. Yang, W. Brehm, P. Adelhelm, From lithium-ion to sodium-ion batteries: advantages, challenges, and surprises, Angew. Chem. Int. Ed. 57 (2018) 102–120.
[6] Y. Liang, H. Dong, D. Aurbach, Y. Yao, Current status and future directions of multivalent metal-ion batteries, Nat. Energy 5 (2020) 646–656.
[7] C. Vaalma, D. Buchholz, M. Weil, S. Passerini, A cost and resource analysis of sodium-ion batteries, Nat. Rev. Mater. 3 (2018) 1–11.
[8] Q. Liu, Y. Wang, X. Yang, D. Zhou, X. Wang, P. Jaumaux, F. Kang, B. Li, X. Ji, G. Wang, Rechargeable anion-shuttle batteries for low-cost energy storage, Chem 7 (2021) 1993–2021.
[9] S.K. Sandstrom, X. Chen, X. Ji, A review of halide charge carriers for rocking-chair and dual-ion batteries, Carbon Energy 3 (2021) 627–653.
[10] A.W. Xiao, G. Galatolo, M. Pasta, The case for fluoride-ion batteries, Joule 5 (2021) 2823–2844.
[11] L. Zhang, H. Wang, X. Zhang, Y. Tang, A review of emerging dual-ion batteries: fundamentals and recent advances, Adv. Funct. Mater. 31 (2021) 2010958.
[12] X. Ou, D. Gong, C. Han, Z. Liu, Y. Tang, Advances and prospects of dual-ion batteries, Adv. Energy Mater. 11 (2021) 2102498.
[13] X. Wu, Y. Xu, C. Zhang, D.P. Leonard, A. Markir, J. Lu, X. Ji, Reverse dual-ion battery via a $ZnCl_2$ water-in-salt electrolyte, J. Am. Chem. Soc. 141 (2019) 6338–6344.
[14] F. Chen, Z.Y. Leong, H.Y. Yang, An aqueous rechargeable chloride ion battery, Energy Stor. Mater. 7 (2017) 189–194.
[15] Y. Wang, Y. Zhang, S. Wang, S. Dong, C. Dang, W. Hu, D.Y. Yu, Ultrafast charging and stable cycling dual-ion batteries enabled via an artificial cathode–electrolyte interface, Adv. Funct. Mater. (2021) 2102360.
[16] Y. Wang, Y. Zhang, Q. Duan, P.-K. Lee, S. Wang, Y. Denis, Engineering cathode-electrolyte interface of graphite to enable ultra long-cycle and high-power dual-ion batteries, J. Power Sources 471 (2020) 228466.
[17] X. Hu, F. Chen, S. Wang, Q. Ru, B. Chu, C. Wei, Y. Shi, Z. Ye, Y. Chu, X. Hou, Electrochemical performance of $Sb_4O_5Cl_2$ as a new anode material in aqueous chloride-ion battery, ACS Appl. Mater. Interfaces 11 (2019) 9144–9148.
[18] X. Li, Y. Tang, J. Zhu, H. Lv, Y. Xu, W. Wang, C. Zhi, H. Li, Initiating a room-temperature rechargeable aqueous fluoride-ion battery with long lifespan through a rational buffering phase design, Adv. Energy Mater. 11 (2021) 2003714.
[19] I.A. Rodríguez-Pérez, L. Zhang, J.M. Wrogemann, D.M. Driscoll, M.L. Sushko, K.S. Han, J.L. Fulton, M.H. Engelhard, M. Balasubramanian, V.V. Viswanathan, V. Murugesan, X. Li, D. Reed, V. Sprenkle, M. Winter, T. Placke, Enabling natural graphite in high-voltage aqueous graphite||Zn metal dual-ion batteries, Adv. Energy Mater. 10 (2020) 2001256.
[20] X. Zhao, Z. Zhao, M. Yang, H. Xia, T. Yu, X. Shen, Developing polymer cathode material for the chloride ion battery, ACS Appl. Mater. Interfaces 9 (2017) 2535–2540.
[21] T. Xia, Y. Li, L. Huang, W. Ji, M. Yang, X. Zhao, Room-temperature stable inorganic halide perovskite as potential solid electrolyte for chloride ion batteries, ACS Appl. Mater. Interfaces 12 (2020) 18634–18641.
[22] D. Zhang, H. Nakano, K. Yamamoto, K. Tanaka, T. Yahara, K. Imai, T. Mori, H. Miki, S. Nakanishi, H. Iba, T. Watanabe, T. Uchiyama, K. Amezawa, Y. Uchimoto, Rate-determining process at electrode/electrolyte interfaces for all-solid-state fluoride-ion Batteries, ACS Appl. Mater. Interfaces 13 (2021) 30198–30204.
[23] D. Yu, Q. Zhu, L. Cheng, S. Dong, X. Zhang, H. Wang, N. Yang, Anion solvation regulation enables long cycle stability of graphite cathodes, ACS Energy Lett. 6 (2021) 949–958.
[24] X. Xu, K. Lin, D. Zhou, Q. Liu, X. Qin, S. Wang, S. He, F. Kang, B. Li, G. Wang, Quasi-solid-state dual-ion sodium metal batteries for low-cost energy storage, Chem 6 (2020) 902–918.
[25] Y. Zhang, Y. An, B. Yin, J. Jiang, S. Dong, H. Dou, X. Zhang, A novel aqueous ammonium dual-ion battery based on organic polymers, J. Mater. Chem. A 7 (2019) 11314–11320.
[26] V.K. Davis, C.M. Bates, K. Omichi, B.M. Savoie, N. Momčilović, Q. Xu, W.J. Wolf, M.A. Webb, K.J. Billings, N.H. Chou, Room-temperature cycling of metal fluoride electrodes: liquid electrolytes for high-energy fluoride ion cells, Science 362 (2018) 1144–1148.
[27] X. Hou, Z. Zhang, K. Shen, S. Cheng, Q. He, Y. Shi, D.Y.W. Yu, C.-Y. Su, L.-J. Li, F. Chen, An aqueous rechargeable fluoride ion battery with dual fluoride electrodes, J. Electrochem. Soc. 166 (2019) A2419–A2424.
[28] T. Placke, A. Heckmann, R. Schmuch, P. Meister, K. Beltrop, M. Winter, Perspective on performance, cost, and technical challenges for practical dual-ion batteries, Joule 2 (2018) 2528–2550.
[29] Y. Sui, C. Liu, R.C. Masse, Z.G. Neale, M. Atif, M. AlSalhi, G. Cao, Dual-ion batteries: the emerging alternative rechargeable batteries, Energy Stor. Mater. 25 (2020) 1–32.
[30] K.V. Kravchyk, M.V. Kovalenko, Rechargeable dual-ion batteries with graphite as a cathode: key challenges and opportunities, Adv. Energy Mater. 9 (2019) 1901749.
[31] M.A. Nowroozi, I. Mohammad, P. Molaiyan, K. Wissel, A.R. Munnangi, O. Clemens, Fluoride ion batteries – past, present, and future, J. Mater. Chem. A 9 (2021) 5980–6012.
[32] P. Meister, V. Siozios, J. Reiter, S. Klamor, S. Rothermel, O. Fromm, H.-W. Meyer, M. Winter, T. Placke, Dual-ion cells based on the electrochemical intercalation of asymmetric fluorosulfonyl-(trifluoromethanesulfonyl) imide anions into graphite, Electrochim. Acta 130 (2014) 625–633.
[33] X. Zhao, S. Ren, M. Bruns, M. Fichtner, Chloride ion battery: a new member in the rechargeable battery family, J. Power Sources 245 (2014) 706–711.
[34] F. Gschwind, H. Euchner, G. Rodriguez-Garcia, Chloride ion battery review: theoretical calculations, state of the art, safety, toxicity, and an outlook towards future developments, Eur. J. Inorg. Chem. 2017 (2017) 2784–2799.
[35] X. Zhao, Z. Zhao-Karger, D. Wang, M. Fichtner, Metal oxychlorides as cathode materials for chloride ion batteries, Angew. Chem. Int. Ed. 125 (2013) 13866–13869.
[36] C. Chen, T. Yu, M. Yang, X. Zhao, X. Shen, An all-solid-state rechargeable chloride ion battery, Adv. Sci. 6 (2019) 1802130.
[37] X. Zhao, Z. Zhao-Karger, M. Fichtner, X. Shen, Halide-based materials and chemistry for rechargeable batteries, Angew. Chem. Int. Ed. 59 (2020) 5902–5949.
[38] C. Derrington, A. Lindner, M. O'keeffe, Ionic conductivity of some alkaline earth halides, J. Solid State Chem. 15 (1975) 171–174.
[39] N. Imanaka, K. Okamoto, G.y. Adachi, Water-insoluble lanthanum oxychloride-based solid electrolytes with ultra-high chloride ion conductivity, Angew. Chem. Int. Ed. 41 (2002) 3890–3892.
[40] H. Matsumoto, T. Miyake, H. Iwahara, Chloride ion conduction in $PbCl_2$-PbO system, Mater. Res. Bull. 36 (2001) 1177–1184.
[41] I. Murin, O. Glumov, N. Mel'Nikova, Solid electrolytes with predominant chloride conductivity, Russ. J. Electrochem. 45 (2009) 411–416.
[42] T. Yu, Q. Li, X. Zhao, H. Xia, L. Ma, J. Wang, Y.S. Meng, X. Shen, Nanoconfined iron oxychloride material as a high-performance cathode for rechargeable chloride ion batteries, ACS Energy Lett. 2 (2017) 2341–2348.
[43] P. Gao, M.A. Reddy, X. Mu, T. Diemant, L. Zhang, Z. Zhao-Karger, V.S. Chakravadhanula, O. Clemens, R.J. Behm, M. Fichtner, VOCl as a cathode for rechargeable chloride ion batteries, Angew. Chem. Int. Ed. 55 (2016) 4285–4290.
[44] Q. Yin, D. Rao, G. Zhang, Y. Zhao, J. Han, K. Lin, L. Zheng, J. Zhang, J. Zhou, M. Wei, CoFe–Cl layered double hydroxide: a new cathode material for high-performance chloride ion batteries, Adv. Funct. Mater. 29 (2019) 1900983.
[45] Q. Yin, J. Luo, J. Zhang, S. Zhang, J. Han, Y. Lin, J. Zhou, L. Zheng, M. Wei, Ultralong-life chloride ion batteries achieved by the synergistic contribution of intralayer metals in layered double hydroxides, Adv. Funct. Mater. 30 (2019) 1907448.
[46] Q. Yin, J. Luo, J. Zhang, L. Zheng, G. Cui, J. Han, D. O'Hare, High-performance, long lifetime chloride ion battery using a NiFe–Cl layered double hydroxide cathode, J. Mater. Chem. A 8 (2020) 12548–12555.

[47] L. Wu, Chloride ion conducting polymer electrolytes based on cross- linked PMMA-$PP_{14}Cl$-$PP_{14}TFSI$ ion gels for chloride ion batteries, Int. J. Electrochem. Sci. (2019) 2414–2421.
[48] Z. Zhang, K. Shen, Y. Zhou, X. Hou, Q. Ru, Q. He, C.-y. Su, L. Sun, S.H. Aung, F. Chen, The composite electrode of Bi@carbon-texture derived from metal-organic frameworks for aqueous chloride ion battery, Ionics 26 (2019) 2395–2403.
[49] F. Gschwind, D. Steinle, D. Sandbeck, C. Schmidt, E. von Hauff, Facile preparation of chloride-conducting membranes: first step towards a room-temperature solid-state chloride-ion battery, ChemistryOpen 5 (2016) 525–530.
[50] M. Anji Reddy, M. Fichtner, Batteries based on fluoride shuttle, J. Mater. Chem. A 21 (2011) 17059–17062.
[51] V.K. Davis, C.M. Bates, K. Omichi, B.M. Savoie, N. Momcilovic, Q. Xu, W.J. Wolf, M.A. Webb, K.J. Billings, N.H. Chou, S. Alayoglu, R.K. McKenney, I.M. Darolles, N.G. Nair, A. Hightower, D. Rosenberg, M. Ahmed, C.J. Brooks, T.F. Miller III, R.H. Grubbs, S.C. Jones, Room-temperature cycling of metal fluoride electrodes: liquid electrolytes for high-energy fluoride ion cells, Science 362 (2018) 1144–1148.
[52] L. Liu, L. Yang, M. Liu, X. Wang, X. Li, D. Shao, K. Luo, Z. Luo, G. Chen, A flexible tysonite-type $La_{0.95}Ba_{0.05}F_{2.95}$@ PEO-based composite electrolyte for the application of advanced fluoride ion battery, J. Energy Storage 25 (2019) 100886.
[53] Y. Yifan, G. Yuping, L. Chilin, Progress on fluoride ion shuttle batteries, Energy Storage Sci. Technol. 9 (2020) 217.
[54] I. Mohammad, R. Witter, M. Fichtner, M.A. Reddy, Introducing interlayer electrolytes: toward room-temperature high-potential solid-state rechargeable fluoride ion batteries, ACS Appl. Energy Mater. 2 (2019) 1553–1562.
[55] T. Yoshinari, D. Zhang, K. Yamamoto, Y. Kitaguchi, A. Ochi, K. Nakanishi, H. Miki, S. Nakanishi, H. Iba, T. Uchiyama, T. Watanabe, T. Matsunaga, K. Amezawa, Y. Uchimoto, Kinetic analysis and alloy designs for metal/metal fluorides toward high rate capability for all-solid-state fluoride-ion batteries, J. Mater. Chem. A 9 (2021) 7018–7024.
[56] L. Liu, L. Yang, M. Liu, X. Li, D. Shao, K. Luo, X. Wang, Z. Luo, SnF_2-based fluoride ion electrolytes $MSnF_4$ (M = Ba, Pb) for the application of room-temperature solid-state fluoride ion batteries, J. Alloys Compd. 819 (2020) 152983.
[57] V.K. Davis, S. Munoz, J. Kim, C.M. Bates, N. Momčilović, K.J. Billings, T.F. Miller, R.H. Grubbs, S.C. Jones, Fluoride-ion solvation in non-aqueous electrolyte solutions, Mater. Chem. Front. 3 (2019) 2721–2727.
[58] I. Mohammad, R. Witter, M. Fichtner, M. Anji Reddy, Room-temperature, rechargeable solid-state fluoride-ion batteries, ACS Appl. Energy Mater. 1 (2018) 4766–4775.
[59] H. Bhatia, D.T. Thieu, A.H. Pohl, V.S.K. Chakravadhanula, M.H. Fawey, C. Kubel, M. Fichtner, Conductivity optimization of tysonite-type $La_{1-x}Ba_xF_{3-x}$ solid electrolytes for advanced fluoride ion battery, ACS Appl. Mater. Interfaces 9 (2017) 23707–23715.
[60] L. Zhang, M. Anji Reddy, M. Fichtner, Development of tysonite-type fluoride conducting thin film electrolytes for fluoride ion batteries, Solid State Ionics 272 (2015) 39–44.
[61] C. Rongeat, M.A. Reddy, R. Witter, M. Fichtner, Solid electrolytes for fluoride ion batteries: ionic conductivity in polycrystalline tysonite-type fluorides, ACS Appl. Mater. Interfaces 6 (2014) 2103–2110.
[62] J. Wang, J. Hao, C. Duan, X. Wang, K. Wang, C. Ma, A Fluoride-ion-conducting solid electrolyte with both high conductivity and excellent electrochemical stability, Small 18 (2022) 2104508.
[63] J. Chable, B. Dieudonné, M. Body, C. Legein, M.-P. Crosnier-Lopez, C. Galven, F. Mauvy, E. Durand, S. Fourcade, D. Sheptyakov, Fluoride solid electrolytes: investigation of the tysonite-type solid solutions $La_{1-x}Ba_xF_{3-x}$ ($x < 0.15$), Dalton Trans. 44 (2015) 19625–19635.
[64] I. Mohammad, J. Chable, R. Witter, M. Fichtner, M.A. Reddy, Synthesis of fast fluoride-ion-conductive fluorite-type $Ba_{1-x}Sb_xF_{2+x}$ (0.1 </= x </= 0.4): a potential solid electrolyte for fluoride-ion batteries, ACS Appl. Mater. Interfaces 10 (2018) 17249–17256.
[65] G. Karkera, M.A. Reddy, M. Fichtner, Recent developments and future perspectives of anionic batteries, J. Power Sources 481 (2021) 228877.
[66] L. Zhang, M.A. Reddy, P. Gao, T. Diemant, R. Jürgen Behm, M. Fichtner, Study of all solid-state rechargeable fluoride ion batteries based on thin-film electrolyte, J. Solid State Electrochem. 21 (2016) 1243–1251.
[67] H. Konishi, T. Minato, T. Abe, Z. Ogumi, Electrochemical performance of a lead fluoride electrode mixed with carbon in an electrolyte containing triphenylboroxine as an anion acceptor for fluoride shuttle batteries, Mater. Chem. Phys. 226 (2019) 1–5.
[68] H. Konishi, T. Minato, T. Abe, Z. Ogumi, Influence of electrolyte composition on the electrochemical reaction mechanism of bismuth fluoride electrode in fluoride shuttle battery, J. Phys. Chem. C 123 (2019) 10246–10252.
[69] H. Konishi, T. Minato, T. Abe, Z. Ogumi, Reactivity of the anion acceptor in electrolyte: an important factor in achieving high electrochemical performance of a lead (II) fluoride electrode in a fluoride shuttle battery, J. Electroanal. Chem. 871 (2020) 114103.
[70] K.-i. Okazaki, Y. Uchimoto, T. Abe, Z. Ogumi, Charge–discharge behavior of bismuth in a liquid electrolyte for rechargeable batteries based on a fluoride shuttle, ACS Energy Lett. 2 (2017) 1460–1464.
[71] J.H. Clark, Fluoride ion as a base in organic synthesis, Chem. Rev. 80 (1980) 429–452.
[72] H. Konishi, T. Minato, T. Abe, Z. Ogumi, Improvement of cycling performance in bismuth fluoride electrodes by controlling electrolyte composition in fluoride shuttle batteries, J. Appl. Electrochem. 48 (2018) 1205–1211.
[73] A.C. Kucuk, T. Minato, T. Yamanaka, T. Abe, Effects of LiBOB on salt solubility and BiF_3 electrode electrochemical properties in fluoride shuttle batteries, J. Mater. Chem. A 7 (2019) 8559–8567.
[74] A.C. Kucuk, T. Yamanaka, T. Minato, T. Abe, Influence of LiBOB as an electrolyte additive on the performance of BiF_3/C for fluoride shuttle batteries, J. Electrochem. Soc. 167 (2020) 120508.
[75] T. Yamanaka, A.C. Kucuk, Z. Ogumi, T. Abe, Evolution of fluoride shuttle battery reactions of BiF_3 microparticles in a CsF/LiBOB/tetraglyme electrolyte: dependence on structure, size, and shape, ACS Appl. Energy Mater. 3 (2020) 9390–9400.
[76] A.C. Kucuk, T. Yamanaka, T. Abe, Fluoride shuttle batteries: on the performance of the BiF_3 electrode in organic liquid electrolytes containing a mixture of lithium bis (oxalato) borate and triphenylboroxin, Solid State Ionics 357 (2020) 115499.
[77] A.C. Kucuk, T. Abe, Electrochemical behavior of CuF_2 as reversible cathode in an organic liquid electrolyte for room-temperature fluoride-shuttle batteries, J. Power Sources 496 (2021) 229828.
[78] A.C. Kucuk, T. Abe, Influence of conductive additives on the electrochemical compatibility of cupper fluoride cathode for FSB, J. Electroanal. Chem. 900 (2021) 115744.
[79] X. Jiang, L. Luo, F. Zhong, X. Feng, W. Chen, X. Ai, H. Yang, Y. Cao, Electrolytes for dual-carbon batteries, ChemElectroChem 6 (2019) 2615–2629.
[80] M. Wang, Y. Tang, A Review on the features and progress of dual-ion batteries, Adv. Energy Mater. 8 (2018) 1703320.
[81] A. Heckmann, J. Thienenkamp, K. Beltrop, M. Winter, G. Brunklaus, T. Placke, Towards high-performance dual-graphite batteries using highly concentrated organic electrolytes, Electrochim. Acta 260 (2018) 514–525.
[82] L. Xiang, X. Ou, X. Wang, Z. Zhou, X. Li, Y. Tang, Highly concentrated electrolyte towards enhanced energy density and cycling life of dual-ion battery, Angew. Chem. Int. Ed. 59 (2020) 17924–17930.
[83] Y. Wang, S. Wang, Y. Zhang, P.-K. Lee, D.Y. Yu, Unlocking the true capability of graphite-based dual-ion batteries with ethyl methyl carbonate electrolyte, ACS Appl. Energy Mater. 2 (2019) 7512–7517.
[84] H. Fan, L. Qi, M. Yoshio, H. Wang, Hexafluorophosphate intercalation into graphite electrode from ethylene carbonate/ethylmethyl carbonate, Solid State Ionics 304 (2017) 107–112.
[85] H. Fan, L. Qi, H. Wang, Intercalation behavior of hexafluorophosphate into graphite electrode from propylene/ethylmethyl carbonates, J. Electrochem. Soc. 164 (2017) A2262.
[86] H. Fan, J. Gao, L. Qi, H. Wang, Hexafluorophosphate anion intercalation into graphite electrode from sulfolane/ethylmethyl carbonate solutions, Electrochim. Acta 189 (2016) 9–15.
[87] L. Zhang, J. Li, Y. Huang, D. Zhu, H. Wang, Synergetic effect of ethyl methyl carbonate and trimethyl phosphate on BF_4(-) intercalation into a graphite electrode, Langmuir 35 (2019) 3972–3979.
[88] Y. Wang, J. Li, Y. Huang, H. Wang, Anion storage behavior of graphite electrodes in $LiBF_4$/sulfone/ethyl methyl carbonate solutions, Langmuir 35 (2019) 14804–14811.
[89] W. Wu, Y. Bai, X. Wang, C. Wu, Sulfone-based high-voltage electrolytes for high energy density rechargeable lithium batteries: progress and perspective, Chin. Chem. Lett. 32 (2021) 1309–1315.
[90] J. Seel, J. Dahn, Electrochemical intercalation of PF_6 into graphite, J. Electrochem. Soc. 147 (2000) 892.
[91] W. Zhao, B. Zheng, H. Liu, F. Ren, J. Zhu, G. Zheng, S. Chen, R. Liu, X. Yang, Y. Yang, Toward a durable solid electrolyte film on the electrodes for Li-ion batteries with high performance, Nano Energy 63 (2019) 103815.
[92] Z. Chen, Y. Tang, X. Du, B. Chen, G. Lu, X. Han, Y. Zhang, W. Yang, P. Han, J. Zhao, G. Cui, Anion solvation reconfiguration enables high-voltage carbonate electrolytes for stable Zn/graphite cells, Angew. Chem. Int. Ed. 59 (2020) 21769–21777.
[93] Y. Wang, Y. Zhang, S. Dong, W. Zhou, P.K. Lee, Z. Peng, C. Dang, P.H.L. Sit, J. Guo, D.Y. Yu, An all-fluorinated electrolyte toward high voltage and long cycle performance dual-ion batteries, Adv. Energy Mater. (2022) 2103360.
[94] J.A. Read, A.V. Cresce, M.H. Ervin, K. Xu, Dual-graphite chemistry enabled by a high voltage electrolyte, Energy Environ. Sci. 7 (2014) 617–620.
[95] Y. Abu-Lebdeh, I. Davidson, High-voltage electrolytes based on adiponitrile for Li-ion batteries, J. Electrochem. Soc. 156 (2009) A60–A65.
[96] X. Tong, X. Ou, N. Wu, H. Wang, J. Li, Y. Tang, High oxidation potential ≈6.0 V of concentrated electrolyte toward high-performance dual-ion battery, Adv. Energy Mater. 11 (2021) 2100151.
[97] J. Wu, X. Wang, Q. Liu, S. Wang, D. Zhou, F. Kang, D. Shanmukaraj, M. Armand, T. Rojo, B. Li, G. Wang, A synergistic exploitation to produce high-voltage quasi-solid-state lithium metal batteries, Nat. Commun. 12 (2021) 5746.
[98] S. Rothermel, P. Meister, G. Schmuelling, O. Fromm, H.-W. Meyer, S. Nowak, M. Winter, T. Placke, Dual-graphite cells based on the reversible intercalation of bis(trifluoromethanesulfonyl)imide anions from an ionic liquid electrolyte, Energy Environ. Sci. 7 (2014) 3412–3423.
[99] G.A. Elia, U. Ulissi, S. Jeong, S. Passerini, J. Hassoun, Exceptional long-life performance of lithium-ion batteries using ionic liquid-based electrolytes, Energy Environ. Sci. 9 (2016) 3210–3220.
[100] M. Nádherná, J. Reiter, J. Moškon, R. Dominko, Lithium bis (fluorosulfonyl) imide–$PYR_{14}TFSI$ ionic liquid electrolyte compatible with graphite, J. Power Sources 196 (2011) 7700–7706.
[101] A. Lewandowski, A. Świderska-Mocek, Properties of the lithium and graphite–lithium anodes in N-methyl-N-propylpyrrolidinium bis (trifluoromethanesulfonyl) imide, J. Power Sources 194 (2009) 502–507.

[102] Y. Fu, C. Chen, C. Qiu, X. Ma, Vinyl ethylene carbonate as an additive to ionic liquid electrolyte for lithium ion batteries, J. Appl. Electrochem. 39 (2009) 2597–2603.
[103] J. Fan, Z. Zhang, Y. Liu, A. Wang, L. Li, W. Yuan, An excellent rechargeable $PP_{14}TFSI$ ionic liquid dual-ion battery, Chem. Commun. 53 (2017) 6891–6894.
[104] Y. Yamada, J. Wang, S. Ko, E. Watanabe, A. Yamada, Advances and issues in developing salt-concentrated battery electrolytes, Nat. Energy 4 (2019) 269–280.
[105] K.V. Kravchyk, P. Bhauriyal, L. Piveteau, C.P. Guntlin, B. Pathak, M.V. Kovalenko, High-energy-density dual-ion battery for stationary storage of electricity using concentrated potassium fluorosulfonylimide, Nat. Commun. 9 (2018) 4469.
[106] G. Chen, F. Zhang, Z. Zhou, J. Li, Y. Tang, A flexible dual-ion battery based on PVDF-HFP-modified gel polymer electrolyte with excellent cycling performance and superior rate capability, Adv. Energy Mater. 8 (2018) 1801219.
[107] D. Xie, M. Zhang, Y. Wu, L. Xiang, Y. Tang, A flexible dual-ion battery based on sodium-ion quasi-solid-state electrolyte with long cycling life, Adv. Funct. Mater. 30 (2020) 1906770.
[108] J. Zhu, Y. Xu, Y. Fu, D. Xiao, Y. Li, L. Liu, Y. Wang, Q. Zhang, J. Li, X. Yan, Hybrid aqueous/nonaqueous water-in-bisalt electrolyte enables safe dual ion batteries, Small 16 (2020) e1905838.
[109] J.M. Wrogemann, S. Künne, A. Heckmann, I.A. Rodríguez-Pérez, V. Siozios, B. Yan, J. Li, M. Winter, K. Beltrop, T. Placke, Development of safe and sustainable dual-ion batteries through hybrid aqueous/nonaqueous electrolytes, Adv. Energy Mater. 10 (2020) 1902709.
[110] H. Jiang, Z. Wei, L. Ma, Y. Yuan, J.J. Hong, X. Wu, D.P. Leonard, J. Holoubek, J.J. Razink, W.F. Stickle, F. Du, T. Wu, J. Lu, X. Ji, An aqueous dual-ion battery cathode of Mn_3O_4 via reversible insertion of nitrate, Angew. Chem. Int. Ed. 58 (2019) 5286–5291.
[111] C. Yang, J. Chen, X. Ji, T.P. Pollard, X. Lü, C.-J. Sun, S. Hou, Q. Liu, C. Liu, T. Qing, Y. Wang, O. Borodin, Y. Ren, K. Xu, C. Wang, Aqueous Li-ion battery enabled by halogen conversion–intercalation chemistry in graphite, Nature 569 (2019) 245–250.
[112] Z.A. Zafar, G. Abbas, K. Knizek, M. Silhavik, P. Kumar, P. Jiricek, J. Houdková, O. Frank, J. Cervenka, Chaotropic anion based “water-in-salt” electrolyte realizes a high voltage Zn–graphite dual-ion battery, J. Mater. Chem. 10 (2022) 2064–2074.
[113] J. Ge, X. Yi, L. Fan, B. Lu, An all-organic aqueous potassium dual-ion battery, J. Energy Chem. 57 (2021) 28–33.
[114] Q. Nian, S. Liu, J. Liu, Q. Zhang, J. Shi, C. Liu, R. Wang, Z. Tao, J. Chen, All-climate aqueous dual-ion hybrid battery with ultrahigh rate and ultralong life performance, ACS Appl. Energy Mater. 2 (2019) 4370–4378.
[115] H. Glatz, E. Lizundia, F. Pacifico, D. Kundu, An organic cathode based dual-ion aqueous zinc battery enabled by a cellulose membrane, ACS Appl. Energy Mater. 2 (2019) 1288–1294.
[116] Q. Guo, K.-i. Kim, H. Jiang, L. Zhang, C. Zhang, D. Yu, Q. Ni, X. Chang, T. Chen, H. Xia, X. Ji, A High-potential anion-insertion carbon cathode for aqueous zinc dual-ion battery, Adv. Funct. Mater. 30 (2020) 2002825.
[117] H. Li, T. Kurihara, D. Yang, M. Watanabe, T. Ishihara, A novel aqueous dual-ion battery using concentrated bisalt electrolyte, Energy Stor. Mater. 38 (2021) 454–461.
[118] Q. Guo, K.-I. Kim, S. Li, A.M. Scida, P. Yu, S.K. Sandstrom, L. Zhang, S. Sun, H. Jiang, Q. Ni, Reversible insertion of I–Cl interhalogen in a graphite cathode for aqueous dual-ion batteries, ACS Energy Lett. 6 (2021) 459–467.
[119] C. Zhang, W. Ma, C. Han, L.-W. Luo, A. Daniyar, S. Xiang, X. Wu, X. Ji, J.-X. Jiang, Tailoring the linking patterns of polypyrene cathodes for high-performance aqueous Zn dual-ion batteries, Energy Environ. Sci. 14 (2021) 462–472.
[120] K.i. Kim, L. Tang, J.M. Muratli, C. Fang, X. Ji, A graphite||PTCDI aqueous dual-ion battery, ChemSusChem 15 (2022) e202102394.
[121] Z. Zhang, X. Hu, Y. Zhou, S. Wang, L. Yao, H. Pan, C.-Y. Su, F. Chen, X. Hou, Aqueous rechargeable dual-ion battery based on fluoride ion and sodium ion electrochemistry, J. Mater. Chem. A 6 (2018) 8244–8250.
[122] L. Suo, O. Borodin, T. Gao, M. Olguin, J. Ho, X. Fan, C. Luo, C. Wang, K. Xu, “Water-in-salt” electrolyte enables high-voltage aqueous lithium-ion chemistries, Science 350 (2015) 938–943.